International Journal of Earth Sciences
https://doi.org/10.1007/s00531-018-1670-2

ORIGINAL PAPER

Possible solutions to several enigmas of Cretaceous climate

William W. Hay[1] · Robert M. DeConto[2] · Poppe L. de Boer[3] · Sascha Flögel[4] · Ying Song[5] · Andrei Stepashko[6]

Received: 24 August 2018 / Accepted: 23 November 2018

Abstract
The nature of the warm climates of the Cretaceous has been enigmatic since the first numerical climate models were run in the late 1970s. Quantitative simulations of the paleoclimate have consistently failed to agree with information from plant and animal fossils and climate sensitive sediments. The 'cold continental interior paradox' (first described by DeConto et al. in Barrera E, Johnson C (eds) Evolution of the Cretaceous Ocean/climate system, vol 332. Geological Society of America Special Paper, Boulder, pp 391–406, 1999), has been an enigma, with extensive continental interiors, especially in northeast Asia, modeled as below freezing in spite of plant and other evidence to the contrary. We reconsider the paleoelevations of specific areas, particularly along the northeastern Siberian continental margin, where paleofloras indeed indicate higher temperatures than suggested by current climate models. Evidence for significant masses of ice on land during even the otherwise warmest times of the Cretaceous is solved by reinterpretation of the $\delta^{18}O$ record of fossil plankton. The signal interpreted as an increase in ice volume on land is the same as the signal for an increase in the volume of groundwater reservoirs on land. The problem of a warm Arctic, where fossil floras indicate that they never experienced freezing conditions in winter, could not be solved by numerical simulations using higher CO_2 equivalent greenhouse gas concentrations. We propose a solution by assuming that paleoelevations were less than today and that there were much more extensive wetlands (lakes, meandering rivers, swamps, bogs) on the continents than previously assumed. Using ~ $8 \times CO_2$ equivalent greenhouse gas concentrations and assuming 50–75% water surfaces providing water vapor as a supplementary greenhouse gas on the continents reduces the meridional temperature gradients. Under these conditions the equatorial to polar region temperature gradients produce conditions compatible with fossil and sedimentological evidence.

Keywords Cretaceous climate · Paleogeography · Paleotopography · Warm Arctic · Climate models

Introduction

Deposits of Mesozoic and Cenozoic age record an important part of the long term plate tectonic cycle (i.e., 'Wilson Cycle' of Dewey and Burke 1974). The late Paleozoic assembly of the continental blocks into a single giant continent began with the union of Gondwana and Laurasia, which was completed about 250 Ma, forming Pangaea (Rogers and Santosh 2013). The final assembly of Pangaea coincided with the end of the Paleozoic Era. Before its breakup at the end of the Triassic Pangaea was a high and dry continent. Southam and Hay (1981), based on sediment offloaded onto passive continental margins during the Mesozoic and Cenozoic, estimated its average elevation to have been of the order of 1500 m—almost twice that of the modern continents.

The initial breakup of the supercontinent began as uplift, with subsequent rifting between North America and Eurasia during the later Triassic (Hay et al. 1982). Actual separation

✉ William W. Hay
whay@gmx.de

[1] Department of Geological Sciences, University of Colorado at Boulder, 2045 Windcliff Dr., Estes Park, CO 80517, USA

[2] Department of Geosciences, University of Massachusetts-Amherst, Amherst, MA 01003, USA

[3] Sedimentology Group, Department of Earth Sciences, University of Utrecht, P.O. 80.115, 3508 TC Utrecht, The Netherlands

[4] GEOMAR Helmholtz Centre for Ocean Research Kiel, Wischhofstr. 1-3, 24148 Kiel, Germany

[5] Department of Geology, China University of Petroleum (East China), Qingdao, China

[6] Far East Division, Kosygin Institute of Tectonics and Geophysics, Russian Academy of Sciences, Kim Yu Chen st., 65, Khabarovsk 680000, Russia

Published online: 18 December 2018

of North America and Eurasia occurred at about 175 Ma, during the Middle Jurassic (Greiner and Neugebauer 2013; Neugebauer and Greiner 2014).

Fragmentation of Pangaea into smaller blocks continued through the rest of the Jurassic and Early Cretaceous, reaching a maximum dispersion during the Mid-Cretaceous. Major collisions between the 'drifting' blocks began during the Late Cretaceous and have continued throughout the Cenozoic. As separation into smaller blocks occurred, continental relief declined, reaching a minimum in the Mid-Cretaceous while oceanic relief reached a maximum (Müller et al. 2008). Erosion rates, estimated from sediment accumulations (Wold and Hay 1993; Ronov 1993, 1994; Hay 1994), indicate that the Cenozoic subduction of young ocean crust and the collision of India with Asia have produced what is now the second greatest topographic relief of the Phanerozoic, but now concentrated in one small area. The Mid-Cretaceous and Quaternary thus represent two extremes for Earth's climate system.

In this paper, we consider the conditions on Earth's land areas during the very warm Mid-Cretaceous period of minimum topographic relief. Specifically, we investigate the 'cold continental interior paradox' (DeConto et al. 1999), the idea of regional glaciers or ice sheets during this episode of global warmth, and explore the implications of lesser meridional temperature gradients.

The late Mesozoic has long been regarded as the classic time of warm Earth 'greenhouse' conditions, with global temperatures and climate equability reaching their maxima. There may have even been 'hothouse' episodes during the Mid-Cretaceous when the Earth and even mid-depth ocean waters became extremely warm (Norris et al. 2002; Bice and Norris 2002; Bice et al. 2003, 2006; Kidder and Worsley 2010, 2012). One of these hothouse episodes coincided with the Mid-Cretaceous topographic minimum, extremely high sea level and large-scale deposition of black shales (OAE2).

Attempts to investigate Mesozoic climates using numerical general circulation models began in the late 1970s. Barron et al. (1981a, b), Barron (1983) and Barron and Washington (1982, 1984) used NCAR's CCM1 numerical climate model to explore the effects of different variables, such as topography, continental position, and sea level changes to determine the cause of Cretaceous warmth. None of these were adequate to explain the warm climate. Subsequent experiments by Barron and Washington (1985) showed that higher levels of atmospheric CO_2 provided both the overall warmer climate and reduced meridional temperature gradient required as a first approximation solution to the problem. Since then higher levels of atmospheric CO_2 have become a standard initial condition in numerical climate models to explain the equable climates of the later Mesozoic (Barron et al. 1993a, b, 1995; Schneider et al. 1985; Sloan and Barron 1990). Moreover, the estimates of past levels of atmospheric CO_2 based on data from sediment masses (Budyko and Ronov 1979, 1987; Budyko et al. 1985), proxies (Arthur et al. 1985; Retallack 2001; Royer et al. 2001; Chen et al. 2001; Sellwood and Valdes 2006; Wan et al. 2011; Wang et al. 2014; Barclay and Wing 2016), and modelling (Berner and Kothavala 2001; Wallmann 2001; Hansen and Wallmann 2003) are sometimes contradictory and ambiguous (Veizer et al. 2000; Royer et al. 2001; Hay 2016).

Many of the numerical climate simulations for the Cretaceous run to date (Barron and Washington 1984; Barron et al. 1995; Sellwood and Valdes 2006) have used '4 × present day' atmospheric CO_2 concentrations whereby 'present day' was taken to be the 340 ppm level of 1980; $4 \times 340 = 1360$ ppm: note that this was already significantly higher than the pre-industrial level of about 270 ppm. Others have experimented with different values—DeConto et al. (1999) used 1230 ppm and 2500 ppm; DeConto et al. (2000a, b) used 1680 ppm; Donnadieu et al. (2006) used 1120 ppm, while Floegel et al. (2005) used 1860 ppm. Bice and Norris (2002) showed that CO_2 concentrations of 4500 ppm or more might be required to simulate tropical and temperate sea surface temperatures of 30 °C or more indicated by proxy data, which are currently under debate. Niezgodzki et al. (2017) produced a new series of simulations of the Late Cretaceous climate using the Maastrichtian paleotopography and paleobathymetry of Markwick and Valdes (2004), comparing the results with the data from both marine and non-marine proxies cited by Upchurch et al. (2015). Their Fig. 7 shows the modeled zonal mean temperatures with different CO_2 concentrations and different subarctic gateway configurations compared to proxy data. There is a slight misfit between the modeled and proxy temperatures suggesting that another mechanism is needed to smooth the meridional temperature gradient.

Atmospheric CO_2 concentrations calculated from geochemical models are thought to vary with increases due to volcanism and decreases due to weathering of silicate rocks (Berner and Kothavala 2001; Wallmann 2001; Hansen and Wallmann 2003; Flögel et al. 2011a, b). However, there are other sinks and sources of CO_2, such as changing solubility with changing ocean water temperatures, variations in global biomass and burial of organic matter. These are an order of magnitude, or more, greater than the amount of CO_2 in the atmosphere.

The idea that changes in high-latitude vegetation might significantly modify the meridional temperature gradient was introduced by Otto-Bliesner and Upchurch (1997). They found that specifying high-latitude low-albedo deciduous forests in a Late Maastrichtian (66 Ma) simulation raised the regional temperatures by 2.2 °C.

Today, and probably throughout Earth history, water vapor has been the most important greenhouse gas. Its concentration above a water surface depends on temperature,

approximately doubling with every 10 °C increase. Prior to the industrial revolution it was about four times as effective a greenhouse gas as CO_2. However, over land its concentration depends on how much is advected from the ocean, the extent of open water surfaces such as lakes, rivers and swamps, and the rate of transpiration by plants. These complexities have commonly been generalized in climate models to be analogous to modern conditions, and are, as will be discussed below, likely underestimated.

There are other natural greenhouse gases, such as methane (CH_4) and nitrous oxide (N_2O) that are not normally considered directly in numerical climate models. DeConto (2012a, b) has used the term 'CO_2 equivalent' to include the effects of these other gases. As discussed below, actual CO_2 concentrations may have been only a fraction of the 'CO_2 equivalent' greenhouse levels. This would explain some of the apparent discrepancies between proxy evidence and geochemical model hindcasts.

Despite the sophistication of numerical climate models, there have been some problems that have defied solution: the 'cold continental interior paradox,' the idea of glaciation during the warmest time of Cretaceous and the problem of survival of reptiles through below-freezing temperatures during the polar nights.

The warm polar regions problem

The idea that the polar regions were warmer than today goes back to Charles Lyell, who in 1837 published a report on the sedimentary deposits of the Danish islands of Seeland and Möen. He believed that the chalk of Britain and Denmark must have been deposited in tropical seas. In the 1850 edition of his *Principles of Geology* he postulated that the continents had a different configuration during the Cretaceous, which allowed the polar regions to become warmer.

In 1870 Adolf Erik Nordenskiöld, on an expedition to find a northwest passage from the Atlantic to the Pacific through the Arctic, collected a Cretaceous flora on the Nûgssuaq Peninsula on the West Greenland coast north of Disco Island, at a latitude of about 70.5°N (Nordenskiöld 1870, 1872). Among the fossils were remains of tropical breadfruit trees. A more detailed discussion of the flora is given in Koch (1964).

Evidence from the northern polar regions is now much more substantial. Tarduno et al. (1998) have described a Mid-Cretaceous (92–86 Ma) vertebrate assemblage from Axel Heiberg Island in the Canadian Arctic. The paleolatitude of the site is given as 72° ± 4°N. The assemblage includes large (2.4 m long) champsosaurs, extinct crocodile-like reptiles, implying that the mean annual temperature exceeded 14 °C and was above freezing during the polar night.

Spicer and Parrish (1987) and Parrish and Spicer (1988) described paleofloras from the North Slope of Alaska (ca. 80°N paleolatitude) which they believed indicate a mean annual temperature of 14 °C during the Coniacian (~ 88 Ma).

Much more detailed evidence has come from paleobotanical studies based on CLAMP (Climate Leaf Analysis Multivariate Program) analysis of fossil leaf assemblages (Wolfe 1993, 1995). Since then many studies have used CLAMP to estimate mean annual, warm month mean, and cold month mean temperatures as well as seasonal rainfall. Based on paleofloristic analysis, Herman (1994) reviewed the paleofloral evidence for warm temperatures in the Russian Arctic. Herman and Spicer (1996) cite Coniacian cold month mean temperatures on Alaska's North Slope as 5.7 °C, on Kamchatka as 0 °C, and Turonian cold month mean temperatures on Kamchatka as − 3.8 °C, and 0.0 °C on Novaya Siber' Island. In an extensive discussion of the Cretaceous flora of the Anadyr-Koryak subregion (North-Eastern Russia), Herman (1999a, b) presented an extensive account of Russian Cretaceous paleofloras but did not discuss paleotemperatures. Herman and Spicer (2010) in a more detailed discussion of the paleofloras of the Novaya Sibirsk Islands conclude that the Turonian cold month mean temperature was + 1.1 ± 3.8 °C. At that time the locality was within 900 km of the North Pole.

Spicer and Herman (2010) present an extensive review and discussion of the paleofloral evidence for a warm Arctic climate during much of the Cretaceous. They estimate that Mid-Cretaceous Arctic Ocean coastal environments had a mean annual temperature of 6.3° ± 2.2°, a warm month mean of 14.5° ± 3.1 °C, and a cold month mean no colder than − 2.0° ± 3.9 °C.

Table 1 (adapted from Table 1 in Spicer and Herman 2010) shows the temperatures, based on CLAMP analysis, for paleofloras from specific Arctic localities.

The evidence that coastal temperatures on land were above freezing during the polar night raises an intriguing problem and offers a clue to Mid-Cretaceous paleoclimatology—how large must the greenhouse effect be to prevent the Arctic Ocean from freezing over during the polar night? During the Mid-Cretaceous the Arctic Ocean was largely isolated from the lower latitude oceans and there is evidence that its surface waters had a salinity lower than the Panthalassic or early North Atlantic Ocean (Hay et al. 1993). Its salinity was probably below 24.7‰, so that at temperatures below 4 °C it would have behaved like a fresh water lake, with a relatively thin colder surface layer that apparently did not freeze.

Studies of Antarctic paleofloras and their paleoclimatic implications are in an early stage (Poole 2000; Poole and Francis 2000; Poole et al. 2000; Cantrill and Hunter 2005; Poole and Cantrill 2006; Francis et al. 2006; Iglesias et al. 2007; Manfroi et al. 2015). Information from plants is

Table 1 Paleoflora locations, ages, MAT (mean annual temperature), WMMT (warm month mean temperature), CMMT (cold month mean temperature), and paleolatitudes

Paleoflora location	Age stage	Age (Ma)	MAT (°C)	WMMT (°C)	CMMT (°C)	Paleolatitude (°N)
N. Alaska	Coniacian	88	13.3	19.1	7.9	80
Nov. Sibir	Turonian	90	9.2	17.2	1.1	82
Yukon	Turonian	90	14.3	21.1	8	73
Vilui B	Cenomanian	95	12.8	21	5.3	68
Grebenka	Cenomanian	98	12.9	20.8	5.9	81
Kamchatka	Turonian	90	7.7	17.7	− 2.4	72
Kamchatka	Coniacian	88	9.6	18.3	1.1	72
Arman R	Coniacian	88	8.2	18.7	− 2.0	68
Tylpegyrgynai	Coniacian	88	8.4	18.8	− 1.6	79
Average	Mid-Cretaceous	90.6	10.7	19.2	4.9	75.0

mostly from the Antarctic Peninsula and adjacent islands in the form of fossil wood with tree-rings. On the basis of these early studies, Francis and Poole (2002) estimate Mid-Cretaceous mean annual temperatures to be about 17–20 °C. There are no estimates for minimum (winter) temperatures.

Other evidence concerning Mid-Cretaceous paleotemperatures from the Antarctic is indirect, based on evidence that the migration of South American dinosaurs, not known from Africa, to Madagascar must have been via Antarctica (Krause et al. 1999, 2006). It seems unlikely that the animals could have covered this long distance in a single polar summer season, suggesting that temperatures were above freezing during the polar winter.

The cold continental interior paradox

The term 'cold continental interior paradox' was introduced by DeConto et al. (1999) to highlight the problem that in early models the interiors of large continental areas would go below 0 °C although the polar regions remained free of perennial ice. Figure 1 shows the nature of the problem. It is a numerical model simulation of winter temperatures for the Lower Turonian produced by Flögel (2001) using GENESIS (Thompson and Pollard 1995a, b), based on a paleogeographic map prepared by Alexander Balukhovsky and Areg Migdisov (Balukhovsky et al. 2004). The simulation assumed a circular orbit, with a solar constant of 98.62% (1346.2 W/m^2) of the present value of 1365 W/

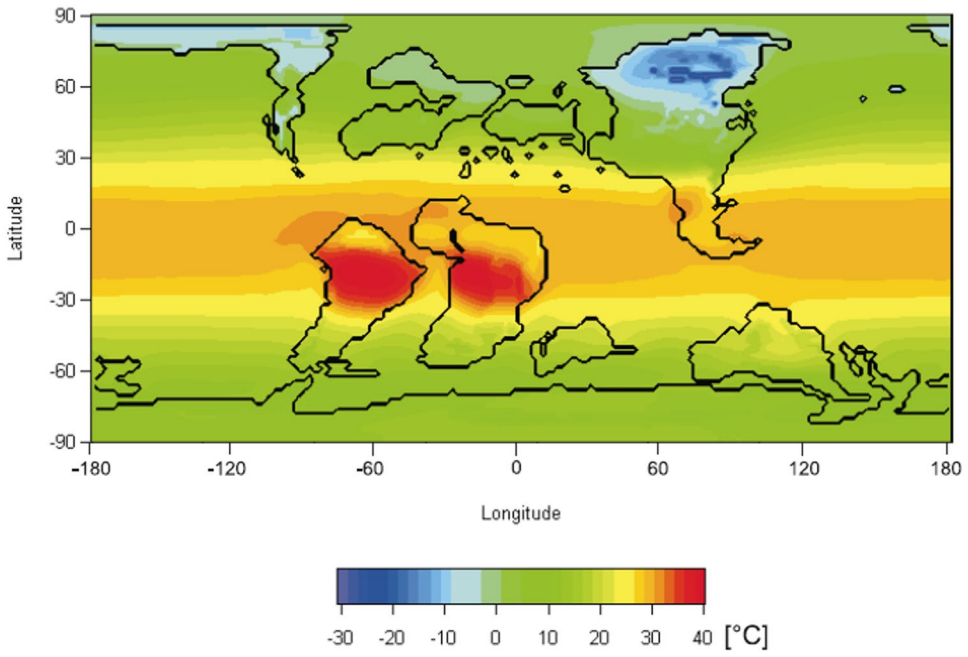

Fig. 1 Numerical simulation of December–January–February temperatures for the Early Turonian (~92 Ma), showing the 'cold continental interior paradox' (from Flögel 2001)

m^2. Atmospheric CO_2 was specified as 1881.6 ppm, 6x the assumed preindustrial level of 313.6 ppm.

A partial solution to the problem was found when C_4 plants, which did not become widespread until the Miocene, were deleted from the vegetation component of the model (DeConto 1996; DeConto et al. 1998, 1999; Upchurch et al. 1998, 1999). This solved part but not all of the problems. Subsequent studies found a major discrepancy between the temperatures indicated by rich fossil plant assemblages known as the Grebenka flora from northeastern Siberia (Herman 1999a, b; Spicer et al. 2002, 2008; Spicer and Herman 2010) and numerical simulations of the contemporary climate (Fig. 1). The flora is preserved in floodplain deposits of the Albian–Cenomanian Krivorechenskaya Formation which occur along and near the banks of the Grebenka River, a tributary of the Anadyr River. The paleoflora is dominated by angiosperms, with lesser numbers of conifers, ferns and other plant groups (Spicer et al. 2002). Multivariate analysis of the leaf physiognomies indicates that the plants experienced a mean annual temperature of 13.0 ± 1.8 °C and a cold month mean temperature of 5.5 ± 3.3 °C (Spicer et al. 2008). The paleolatitude of the fossil sites is about 72°N, well north of the Arctic Circle. The numerical age of the paleofloral assemblages has been determined to be Mid-Cretaceous (96.5 Ma, mid-Cenomanian), based on $^{40}Ar/^{39}Ar$ analyses of associated volcaniclastics (Spicer et al. 2002).

More recently, numerical climate simulations for the Mid-Cretaceous (e.g. Sellwood and Valdes 2006) have also produced winter temperatures well below freezing in the Grebenka region. Sewall et al. (2007) showed the critical area to be between 1000 and 1800 m above sea level; a similar elevation had been assumed in all earlier climate simulations. Assuming a lapse rate (decline of temperature with elevation) of 6 °C/km, reducing the elevation to near sea level would almost eliminate the below freezing winter temperatures despite the polar paleolatitude of the fossil site, and explain the floodplain deposits in the Krivorechenskaya Formation.

The Grebenka area is included in the Chukotka region; its topographic history has been discussed by Bely (1997) and it is part of the Pacific-Asia margin affected by major changes in sea-floor spreading rates described by Stepashko (2009) and Song et al. (2015). They indicate that the time of maximum compression and uplift there would have been 88–89 Ma (Coniacian), 8.5–7.5 million years younger than the age of the Cenomanian Grebenka paleofloras. As noted by Hay (2017), the 'cold continental interior paradox' and the according mismatch between the winter temperatures indicated by the paleofloras and climate model simulations appears to be a function of using an incorrect paleotopography as an initial condition for the models. Maximum compression only leads to strong uplift if the subducting slab is young. If it was old even strong compression may not lead to strong uplift.

The Mid-Cretaceous Hadley circulation

The modern atmosphere generally circulates as three cells in each hemisphere: (1) the Hadley cells between the Intertropical Convergence (today about 3°N of the equator) and the Subtropical Highs at about 30°N and S; (2) the Ferrell cells between 30°N and S and roughly 40°–60°N and S depending on the season, and (3) the Polar cells above roughly 40°–60°N and S depending on the season, and the Polar Highs, areas of high atmospheric pressure around the poles. Because the Polar regions have been until recently perennially ice covered forcing Polar highs, this circulation system has been quite stable.

Today, the meridional temperature gradient is almost flat across the equator between the subtropical highs in the northern and southern hemispheres. The gradient increases between the subtropical highs and the high latitudes, with its slope varying in each hemisphere with the distribution of land and with the seasons.

It has been noted that if the polar regions were ice-free, the polar pressure systems should oscillate between highs and lows with the seasons (Hay 2008, 2009—note that the relevant figures in both publications have Earth's position January and July reversed). Because during the later Mesozoic and Cenozoic the North Pole has been covered by water and the South Pole by land, both poles might have had atmospheric highs and lows at the same times. The atmosphere would then circulate with an even number of cells in each hemisphere, depending on interaction between the pressure differences and the Coriolis effect. It is also possible that because of the gentle latitudinal temperature decline at higher latitudes, atmospheric circulation poleward of the Subtropical Highs might simply have been disorganized and chaotic.

Until recently, it was assumed that the Hadley circulation was quite stable, and that even on an Earth free of polar ice the subtropical highs would be close to where they are today, at about 30°N and S. However, there is now evidence that the northern hemisphere desert zones are spreading and migrating northward (DeMeo 1989) and that the Subtropical Highs over the oceans are expanding poleward and moving westward (Li et al. 2011, 2012).

Hasegawa et al. (2012) presented evidence that during the Mid-Cretaceous super greenhouse (Aptian through Early Coniacian; 125–87 Ma) the Hadley circulation shrank, with the descending limbs on land at about 20°N and S latitude. They were able to locate the site of the descending limb of the Hadley Cell in the northern hemisphere by determining divergent paleowind directions in Cretaceous desert regions

of eastern Asia. Their conclusion is that in that region there was a shift in the Hadley downwelling limb, from about 30°N to 15°N. They proposed that this occurs as a sudden jump at a pCO_2 threshold level of about 1000 ppmv.

The relevant paleoenvironmental maps of Chumakov (Chumakov 1995, 2004; Chumakov et al. 1995), reproduced in Hay and Floegel (2012), can be interpreted as supporting the Hasegawa et al. (2012) hypothesis. Flögel's (2001) numerical simulation of December–January–February temperatures for the Early Turonian, shows the warmest southern hemisphere temperatures equatorward of 30°S, also supporting the Hasegawa et al. (2012) hypothesis.

If during the Mid-Cretaceous 'super greenhouse' the subtropical highs migrated equatorward to 15°N and S, this implies a significant redistribution of the atmospheric mass. Today about half of the mass of the Earth's atmosphere is in the Hadley cells; restricting their extent to only 15° in each hemisphere would reduce their mass to about 1/4 that of the total atmosphere.

Glaciation on a Cretaceous warm Earth?

Evidence for the existence of quasi-permanent ice-sheets or glaciers during the Cretaceous rests on one site with direct evidence (Alley and Frakes 2003) and four types of indirect evidence: ice-rafted debris, dropstones, glendonites, and the $\delta^{18}O$ record of oceanic plankton.

Alley and Frakes (2003) described a diamictite, the Livingston Tillite, from the Early Cretaceous (Valanginian-Berriasian) Eromanga Basin sequence in the northern Flinders Range of southern Australia. This would have been at a paleolatitude of ~65°S at the time. They suggested that the glaciation was probably short-lived. Ice-rafted debris and dropstones (Frakes and Francis 1988) and glendonites (DeLurio and Frakes 1999) had previously been described from the region, spanning a time interval from Valanginian to Aptian. The region where these deposits have been reported are associated with pre-rift uplifts associated with the breakup of Gondwana shown in Figs. 2 and 3 (Hay 2008). Such pre-rift uplifts have been discussed by Kinsman (1975) and Hay (1981). They were the primary higher elevation regions during most of the Mesozoic.

Dropstones, isolated pebbles found in fine-grained sediments, do not necessarily indicate glacial ice, they can be dropped from seasonal ice on ponds or the seashore. Pebbles and even large rocks can be carried out to sea entangled in the roots or branches of shrubs or trees (e.g. Fig. 4). Ice-rafted dropstones may not be easily distinguished from pebbles transported entangled in wood if not accompanied by other markers such as glendonites, and thus may have been misinterpreted in the literature.

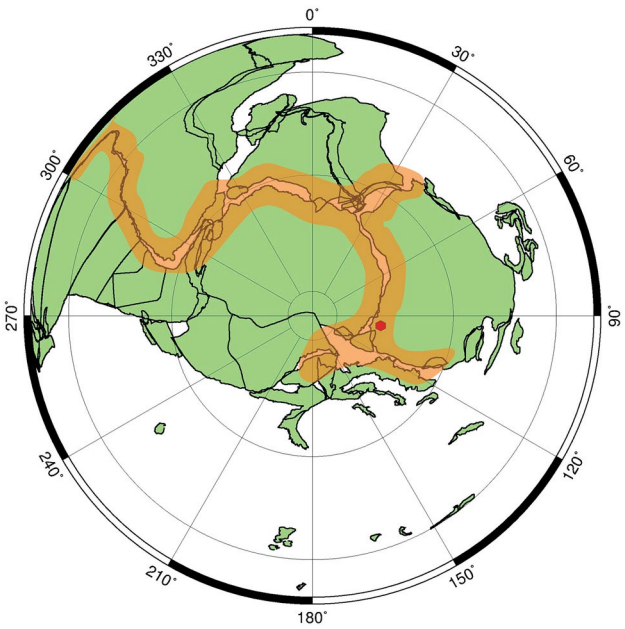

Fig. 2 Ephemeral uplifts associated with the breakup of Gondwana during the Cretaceous, shown on a 140 Ma plate tectonic reconstruction from http://www.odsn.de/odsn/. These uplifts reached their maxima at different times according to the age of separation. The site of the Livingston Tillite (Alley and Frakes 2003) is shown as a red hexagon, clasts in sediment (dropstones) are nearby

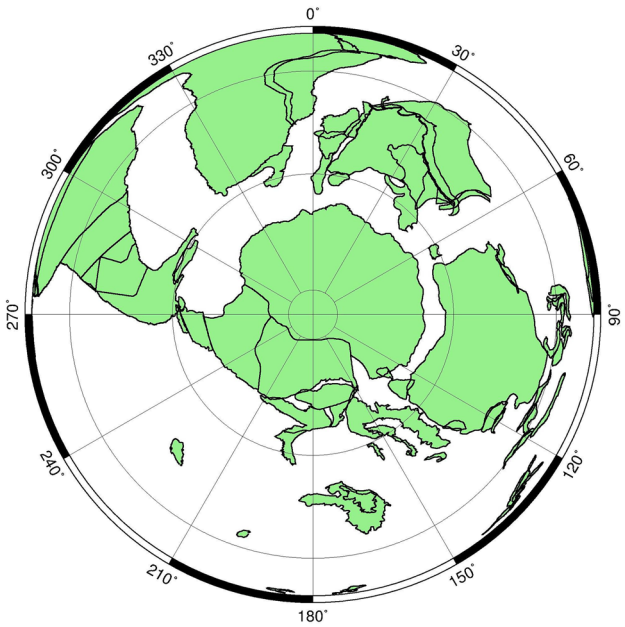

Fig. 3 Breakup of Gondwana at 94 Ma. Plate tectonic reconstruction from http://www.odsn.de/odsn/

Glendonites are anhydrous calcium carbonate pseudomorphs of the monoclinic hydrous calcium carbonate mineral ikaite (Kemper and Schmitz 1981; Suess et al. 1982),

Fig. 4 Pebbles captured in cleared trees and roots, camping site near Rethymnon, Crete, summer 1988 (photo P. L. de Boer). Larger cobbles are up to ~30 cm in length

originally described from the Ika (Ikka) Fjord of Greenland (Pauly 1963). Removed from cold water, ikaite dehydrates to become a more stable carbonate mineral while preserving the monoclinic crystal form. It has generally been accepted as an indicator of very cold-water conditions (Kemper 1987; Greinert and Derkachev 2004; Mutterlose et al. 2008; Price and Nunn 2010; Rogov and Zakharov 2010; Suess 2014; Grasby et al. 2017). However, recently that exclusive interpretation has been called into question with the suggestion that methane seeps and pore water chemistry might also be partially responsible (Selleck et al. 2007; Schultz 2009; Teichert and Luppold 2013).

Flögel et al. (2011a, b) used a series of numerical simulations of Cretaceous climate to investigate whether snowfall and consequent ice formation on Antarctica might account for rapid, low-amplitude Cretaceous sea-level fluctuations. They showed that ice build-up large enough to drive sea level fluctuations on the order of tens of meters within ~20,000 years could occur under the assumption of atmospheric pCO_2 levels < 800 ppm, low insolation, and elevated topography. They showed that initial snow accumulation and consequent growth of Antarctic ice-sheets in the Cretaceous could be attributed to changes in southern hemisphere summer insolation due to reduced orbital eccentricity. However, these models also showed that the buildup of Antarctic ice would require winter temperatures in the higher latitudes of the Northern hemisphere to be below freezing.

Another line of evidence for ice sheets during the Cretaceous comes from interpretation of the $\delta^{18}O$ record of oceanic plankton. During the Quaternary, an increase in $\delta^{18}O$ in ocean plankton occurs as ice sheets grow because water molecules containing the lighter O isotope, ^{16}O, are preferentially evaporated from the ocean surface and become incorporated in snow and ice precipitated over land. It has been assumed that this process has operated consistently throughout geologic time, so that an enrichment of ^{18}O in ocean waters (and oceanic carbonates) indicates storage of ice on land and corresponds to a fall of sea-level.

It has been proposed that there were small ($10–15 \times 10^6$ km^3), ephemeral ice sheets during the Mid-Cretaceous very warm Earth episode (Miller et al. 2003, 2005; Miller 2009) based on interpretation of the $\delta^{18}O$ record of oceanic plankton, with positive $\delta^{18}O$ excursions being interpreted as coinciding with sea level falls. The most likely site for a land area high enough for accommodating ice caps would have been in northeastern Siberia, the region of the 'cold continental interior paradox' and locus of the Grebenka Flora. However, that area is not large enough to accommodate the ice sheet indicated by the $\delta^{18}O$ record.

There is an alternative explanation for sea level rises and falls on a warm ice-free Earth: aquifer eustasy.

The idea of falls and rises of sea level due to the filing and emptying of inshore ground water reservoirs was introduced by Hay and Leslie (1990). Using analysis of the pore space available above sea level for groundwater storage, they concluded filling and emptying the pore space presently available could accommodate 76 m of sea level change before, or 50 m of sea level change. The estimated that for times with significantly larger volumes of sediment above sea level, such as the Cretaceous (Ronov 1982, 1993), the potential for sea level change could have been twice as large. This topic has been further addressed by Jacobs and Sahagian (1993, 1995) and most recently with reference to the Cretaceous by Wagreich et al. (2014, 2016), Sames et al. (2016), Wendler and Wendler (2016) and Wendler et al. (2016). Cretaceous sea level changes are of the order of 30 m (Haq 2014; Hay 2017), well within the possible range suggested by Hay and Leslie (1990) with regularity suggesting a long Milankovitch cycle.

There is no other evidence for glacial ice in the Mid-Cretaceous (Hay 2017). The evidence for extensive glacial ice during the Maastrichtian and Early Cretaceous is in conflict with other evidence for warm sea-surface and land temperature and needs closer examination.

Mid-Cretaceous paleogeography

The history of reconstructions of the topography of continents in the past has been reviewed by Hay et al. (1989). The first global maps were produced by Termier and Termier (1952, 1960) using a modern geographic reference frame and a lot of educated guesswork. In the late 1960s scientists at the Academy of Sciences of the USSR produced four 'lithologic-paleogeographic' atlases which have served as a base for many later studies. The atlas by Armor et al. (1966) deals with the Mesozoic.

The development of a plate tectonic history of the Earth was achieved first through the exploration of possible fits

of the continental blocks (Smith and Briden 1977; Barron et al. 1981a, b), then through reconstruction back to the late Jurassic based on sea floor magnetic anomalies. These have been extended back into the late Precambrian based on paleomagnetic studies from the continents. The improved reconstructions have provided a more sophisticated framework for understanding the major events of our planet's history. Zharkov et al. (1998) produced a set of global lithologic–paleogeographic maps for the Coniacian–Maastrichtian. Over the past decades, the reconstructions have been revised and improved, and Müller et al. (2008a) have proposed reconstructions back to 140 Ma based on the pattern of subducted crust These reconstructions have been especially important in providing a basis for reconstructing past topographies along subduction zones, as discussed below.

Paleotopographic reconstructions

The techniques for reconstructing global paleo-topographies are not exact, and numerical estimates of elevation are rare. For reconstructions of the Mesozoic paleogeography most elevation estimates are ambiguous.

The paleotopographic reconstruction of upland areas shown in the atlases of Armor et al. (1966) and Ronov et al. (1984, 1989) were made by replacement of the sediments surrounding uplifts back onto the areas of erosion and making appropriate isostatic adjustments (Alexander Balukhovsky, Areg Migdisov, personal communications) to estimate the original elevations. The terminology used was simple: platforms of continents—areas of erosion low–high; areas of terrestrial sedimentation or subaerial volcanic activity; seas: shelf seas—deep seas (continental slopes and subocean basins); geosynclines—areas of erosion; areas of terrestrial sedimentation or subaerial volcanic activity; seas, shelf areas; seas, continental slopes and troughs; seas, deep sea areas; orogens—land (mostly mountains) areas of erosion; intermontane and foredeep basins with continental sedimentation and/or subaerial volcanic activity; seas: neritic—deep sea.

The Kazmin and Napatov (1998) atlas for northern Asia, subtitled '*Paleogeographic maps on the palinspastic reconstruction*', distinguishes between the following paleogeographic environments: high mountains and plateaus; moderate mountains and plateaus (from 380 to 240 ma high mountains and plateaus), lowland (hills, plane [=*plain*]), lacustrine–fluvial plane, lagoon, deltaic-shallow marine plane, shelf and other shallow marine basins, continental slope, foot and other deep basins, oceanic floor (abyssal plane).

In their initial suite of maps for the Paleomap Project, Ziegler et al. (1982) distinguished only lowland areas and mountains. For its maps, Chris Scotese's continuation of the Paleomap Project (http://www.scotese.com/) uses the terms deep ocean, shallow seas, lowlands, uplands, and high mountains. Similarly, Ron Blakey's maps at https://deeptimemaps.com/ are qualitative depictions.

The first numerical climate models distinguished only between land and ocean. More sophisticated models require the topography to be specified, with each cell given a numerical elevation. For their global circulation model experiments using NCAR's CCM1, Barron and Washington (1982) used very generalized estimates of Mid-Cretaceous paleotopography with 1 and 2 km contours. In developing more sophisticated numerical paleotopographic depictions, two methodologies have been followed.

Ziegler et al. (1985) used presently exposed rock types to estimate paleoelevations: 0–200 m—coastal plains, lower river systems, delta tops evidenced by alluvial and floodplain complexes, swamps, channel sands; 200–1000 m—inland plains, rift valleys, some forearc ridges evidenced by basalts, lake deposits in grabens, tectonic mélanges; 1000–2000 m island arc peaks, rift shoulders evidenced by andesites/granodiorites and adjacent fanglomerates; 2000–4000 m Andean-type peaks evidenced by andesites/granodiorites in a continental setting; 4000–10,000 m collisional mountains evidenced by high temperature, high pressure metamorphics. This assumes that 'the modern relationship between elevation and tectonics is acceptable for reconstructing past topography (i.e. a uniformitarianist approach)' (Markwick et al. 2000). This technique has been followed for developing a series of paleo-digital elevation models for use with the Hadley Centre coupled ocean–atmosphere model HadCM3 (Markwick and Valdes 2004).

Another method for estimating numerical paleotopography of the continents in the past has been developed by following a few simple rules: topographic highland areas are sites of erosion, so reconstruction of their elevations has been made by determining the volume of sediment eroded from them and replacing it onto the source areas with isostatic adjustment (Hay et al. 1989; Shaw and Hay 1989; Wold et al. 1993). This approach should work well for detrital sediment if the continent itself is not deformed and the original stratigraphic sections eroded did not contain significant amounts of carbonate rock. However, if limestones or dolomites made up a significant part of the rocks they would have been carried in solution by rivers to the sea. Once in the ocean the dissolved carbonate material would eventually be precipitated, usually by organisms, anywhere in the world but mostly in the tropics. A correction for this uncertainty can be approximated by assuming that the stratigraphic section eroded had the same proportion of carbonate to non-carbonate sediment found in sections of those ages still preserved elsewhere on a global scale. The Ronov (1993) data show that for strata older than the Oligocene, the average proportion of carbonate rock in sediments on the continental

blocks is close to 30%. For Oligocene and younger strata, the proportion drops to less than half that value.

Unfortunately, there is no definitive way to interpret the Ronov (1993) sediment mass curve in terms of a numerical average elevation of the continental blocks above sea level at any given time. The rate of erosion is a sporadic process. The mass of the eroded and redeposited sediment depends on the rate of weathering, the state of consolidation of sediments exposed at the surface, the variability of the weather (temperature, rainfall), relief morphology, rivers and glaciers, etc. (Hay and Usselmann 1994; Hay 1998; Leeder 2007). Integrated long-term erosion rates, determined from cosmogenic isotopes such as ^{10}Be, offer a better idea of how and where denudation occurs (Schaller et al. 2001; von Blankenburg 2005) but its half-life is only 1.39 million years.

A problem that has only recently been recognized is that the continental blocks themselves have been significantly warped by convective processes in the Earth's mantle (Conrad 2013; Cloetingh and Haq 2015). Africa rides anomalously high out of the ocean (Hay and Southam 1977) because of unusually warm underlying mantle in the east and south. Continental breakup is a process lasting tens of millions of years, warping the adjacent areas of the continental blocks first upward, and then downward. Hay (1981) proposed a time scale of 100 million years, and geographical scale of 1000 km for this process. Others, such as Kevin Burke (personal communication) have suggested shorter time scales (40 million years) and smaller geographic dimensions (250 km). Furthermore, detrital sediments deposited on the margin of a growing rift shoulder are likely to be recycled back into the rift system, so that their final location and age may be much younger than the time of their original erosion (Hay 1981).

Today Asia, North and South America all are unusually high due to special processes: underthrusting of the Indian block to produce the Tibetan Plateau, and, for the Americas, overriding or proximity of the East Pacific Rise (Harrison et al. 1983). Since the Early Cretaceous, North America has experienced deformation with regional downwarping as the flat-subducting cool Farallon Plate has passed beneath North America (Liu et al. 2008, 2011). The uncertainties become progressively greater back in time, so that pre-Cenozoic reconstructions which may involve indeterminate warping of the continental blocks become numerically ambiguous.

Finally, there is a problem in determining past rates of erosion because virtually all river loads measured since the nineteenth century have been modified by human activity (Hay 1998).

For the numerical climate models of the early Turonian reported by Flögel (2001), Alex Balukhovsky and associates prepared a paleogeographic map using the techniques developed for the Ronov et al. atlases (Balukhovsky et al. 2004). The map distinguished four different topographic levels, which were then assigned numerical values: low lands (0–200 m), low mountains (200–500 m), medium high mountains (500–1000 m) and high mountains (1000–3000 m).

The most detailed topographic reconstruction for climate modeling has been produced by Sewall et al. (2007). They distinguish contours for 0, 200, 400, 600, 800, 1000, 1400, 1800, and 2200 m based on the interpretation of maps produced by the Scotese Paleomap Project (http://www.scotese.com/earth.htm) and Blakey Paleogeography program (http://jan.ucc.nau.edu/rcb7/globaltext2.html) maps. Their Cenomanian–Turonian map shows large areas of central Asia and northeastern Asia with elevations above 1000 m.

Considering the discussions of Bely (1997), Stepashko (2009), Song et al. (2014, 2015) and Hay (2017), we use a new paleotopographic model for the Mid-Cretaceous (94 Ma) climate simulations described below. Note that the continents are fringed by a 0–50 m lowland belt. This reflects the loading of the continental margins by the maximum sea-level transgression which occurred about this time (Hay 2017). The displaced mantle would have migrated underneath the continental blocks as well as beneath the adjacent ocean floor.

Cretaceous versus modern hypsography

Analysis of data on existing sediment masses suggests that the topographic relief of the continents in the late Cenozoic may be quite anomalous. Hay (1994) noted that Holocene and Quaternary sedimentation rates are very different from those of earlier times. This becomes evident when the younger data are compared with Ronov's (1993) compilation of existing volumes and masses of Pliocene–Cambrian sediments.

To compare global sediment masses of past ages it is first necessary to account for losses of sediment along with ocean crust due to subduction of the ocean floor. Accounting for this would be straightforward if there had not been significant variations in the amount of sediment accumulation on the ocean floor. The shift of carbonate sedimentation from the margins of the continental blocks to the deep-sea occurred with the evolution of calcareous nannoplankton and planktonic foraminifera from being shelf-sea dwellers in the Jurassic to becoming inhabitants initially of the upper layers and subsequently the deeper layers of the open ocean during the Cretaceous (Hay 2008). During the Neogene, there has been a major increase in the flux of silicate minerals to the deep sea. Already Donnelly (1982), based on the extensive sediment record that had been assembled by the Deep Sea Drilling Project, reported a six-fold increase in Al_2O_3 that started about 15 million years ago.

We believe that the Cenomanian–Turonian was the time of minimal continental relief during the Phanerozoic, and the time of minimal detrital sediment delivery to the ocean. The climate simulations presented below support the assumption of these extreme conditions.

The modern hypsography is that of NOAA, based on ETOPO1 data and is shown relative to present day sea level. The curve for 94 Ma is based on the relief shown in Fig. 5 relative to the higher sea level (ca. + 250 m) at the time (Haq 2014). Note that although the continental relief at 94 Ma is much less than today, the elevation of the lowland areas of the continent is higher than that of today. This is because of two factors: (1) the continental blocks as a whole are elevated relative to the center of the Earth by the larger mass of water in the oceans which depresses the sea floor and causes flow of asthenospheric material from beneath the oceans to beneath the continental blocks causing them to rise by about 80 m, and (2) the large amounts of sediment lost from the peripheral areas of the modern continents due to the sea level lowstands during Pliocene and Quaternary glaciations—about five times that of pre-glacial mass fluxes (Hay 1994, 1998) (Fig. 6).

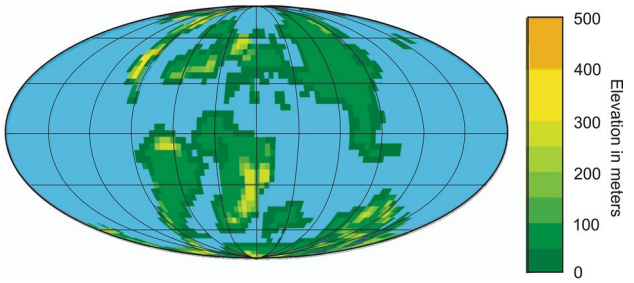

Fig. 5 Paleotopography for 94 Ma (~Cenomanian–Turonian boundary) used for the climate simulations presented below. Mollweide projection

Mesozoic greenhouse gases

Until recently, numerical simulations of Mesozoic climates have only considered the effect of higher concentrations of CO_2. Because of the many interactions with land–sea distribution, plant life and the effect of rising temperatures on the atmospheric concentration of the most important greenhouse gas, H_2O, there are no exact relationships between an increase in atmospheric CO_2 concentration, global temperature, the meridional temperature gradient, and regional temperatures. The relation between CO_2 and temperature is logarithmic (Ramanathan and Vogelmann 1997; Huang and Shahabsdi 2014), but in climate models the effect of increasing CO_2 is commonly explored using doubling of its concentration. Estimates for the effect on global temperatures of doubling the pre-industrial CO_2 concentration range from increases of 1.5 to 4.5 °C with a 'best guess' of 2.5 °C (Houghton et al. 1990; Sellers et al. 1996). Using the NCAR CCM1 to model Mid-Cretaceous climate, Barron and Washington (1994) found that in addition to the effect of changing ice-albedo, paleogeography, paleotopography, and sea-level ($\Sigma = 3.8$ °C), an atmospheric concentration of $4 \times CO_2$ was

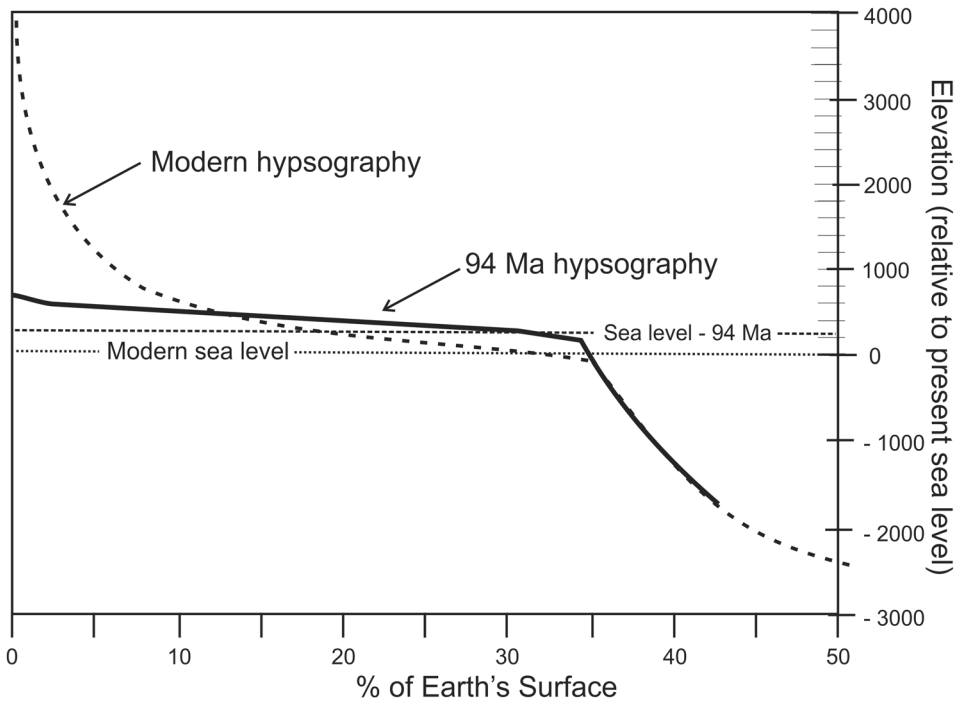

Fig. 6 A comparison of continental hypsography at the Cenomanian–Turonian boundary (94 Ma, solid line) with that of today (dashed line). See text for discussion

required to bring the global mean surface temperature to the 22 °C (+6 °C) required by paleontologic data available at the time.

Recently, Royer et al. (2012) have reported that Earth system climate sensitivity studies suggest that a doubling of CO_2 generally results in a global temperature increase of about 3 °C. However, they noted that the many possible interactions with the other components make this estimate somewhat uncertain.

Recognizing that the assumption that Cretaceous warmth was essentially due to higher CO_2 levels was not realistic, it has been suggested that other factors might be responsible. Sloan and Pollard (1998) suggested that polar stratospheric clouds might enhance polar warming. Kump and Pollard (2008) suggested that the CO_2 greenhouse effect might be enhanced by biologically produced cloud condensation nuclei (CCN) such a dimethylsulfoxide produced by marine plankton.

DeConto et al. (2012a, b) recognized that the ratio of CO_2 to other 'minor' natural greenhouse gases, CH_4 and N_2O, cannot be assumed to have been constant through time. To explore the effects of changing the ratios of these gases they introduced the term $*CO_2$ as the 'equivalent parts per million by volume' mixing ratio (eppmv) for changes in the greenhouse effect with varying atmospheric CO_2 content while also varying the concentrations of CH_4 and N_2O. They presented the results of eight climate model experiments with different combinations of gases.

Sources, sinks, and effectiveness of different greenhouse gases are discussed in Hay (2016). The relative greenhouse potentials of CO_2, CH_4 and N_2O are 1, 23, and 296, respectively. That of water vapor is much less (0.28), but its concentration in the atmosphere can be much greater, as will be discussed below. The lifetimes of molecules of these gases in the atmosphere vary greatly, from thousands to many thousands of years for CO_2, a decade or so for CH_4, and a century or more for N_2O (see discussions in Hay 2016).

The ultimate natural source of CO_2 is thought to be volcanic activity and its ultimate sink to be the weathering of silicate minerals. It is also removed by burial of organic matter in sediments and added by release of that organic matter through weathering and erosion. At present its atmospheric concentration varies by about 1.5% throughout the course of the year due to seasonal changes in vegetation. During the Cretaceous there was a more even distribution of the landmasses in the northern and southern hemispheres, so this annual variation would have been less. CO_2 is the only one of these three natural greenhouse gases whose concentration in the ancient past can be estimated by geochemical modelling and fossil proxies. The biogeochemical models (e.g. Berner and Kothavala 2001) provide a general scheme, but do not include possible excursions due to special events. The proxies include the $\delta^{13}C$ of phytoplankton, the $\delta^{13}C$ of pedogenic carbonates, the $\delta^{13}C$ of the organic remains of phytoplankton, the stomatal density and stomatal index of land plants, the $\delta^{11}B$ of marine calcium carbonate, and the redox chemistry of marine cerium. Unfortunately, they all give different results, some ranging as high as 3000 ppmv (Hay 2017). Royer et al. (2001) review and evaluate these different methods.

Today, methane, CH_4, is produced mostly by decomposition of organic matter by anaerobic bacteria. This process occurs in wetlands, bogs, and in sediments rich in organic matter. Today, a major source is rice paddies. We postulate that natural wetlands were much more extensive in the Cretaceous, emitting more methane into the atmosphere than today. Anaerobic bacteria also live in the digestive tracts of ruminant animals such as cattle, and in the past, dinosaurs. They also occur in the digestive tracts of termites, which use them to digest the wood they eat. Termites were also present in the Cretaceous (Thorne et al. 2000) but their contribution of methane to the Cretaceous atmosphere is difficult to evaluate. Smaller amounts of methane are also emitted from hydrothermal vents along the mid-ocean ridges.

Most of Earth's atmosphere is molecular nitrogen, N_2; it is essentially inert and not readily fixed into the compounds necessary for life on Earth. Natural fixation is through lightning (Hill et al. 1980) and biological fixation through nitrogenase, a process thought to have originated in the Archean (Boyd and Peters 2013). However, most atmospheric N_2O comes from three sources: urea, dung, and soils. That in soils may come from either of the first two or from decomposing plant material and animal remains.

Table 2 shows how different combinations of these three greenhouse gases can combine to produce a total greenhouse effect given in terms of 'CO_2 equivalent'. Following the often-accepted idea that doubling the concentration of a greenhouse gas doubles its effect, the concentrations are shown in terms of 1, 2, 4, 8, and 16 times the estimated preindustrial concentration of each of these gases. Technically, doubling CO_2 does not exactly double its effect because radiative forcing for CO_2 is a logarithmic relationship (Royer et al. 2007). Three different temperature effects for 4 × preindustrial CO_2 are shown because the effect would depend on topographic relief, biome interactions, water surface nature and areas, and possible other factors. The climate classifications (Icehouse, Interglacial, Cool greenhouse, Warm Greenhouse, and Hothouse) are those of Kidder and Worsley (2002). The 'Extreme Hothouse' condition, with global mean temperatures in excess of 40 °C, would be inimical to most plant life and has probably not happened during the Phanerozoic. The first row is for the Last Glacial Maximum, with concentrations based on ice cores.

Table 2 'CO_2 equivalent' greenhouse gas intensities for different combinations of CO_2, CH_4, and N_2O, showing the global climate conditions they would induce, following Kidder and Worsley (2012)

Concentration ppmv (1 = pre-industrial value)						Greenhouse effect: Intensity relative to pre-industrial CO_2				'CO2 equivalent'	Temperature effect with 4 × pre-industrial CO_2			Temperature difference from 15°C		
× CO_2	CO_2	× CH_4	CH_4	× N_2O	N_2O	CO_2	CH_4	N_2O	Total Greenhouse Intensity	Total Greenhouse Intensity / Pre-industrial Greenhouse Intensity	Global T if 4 × CO_2 = 19°C	Global T if 4 × CO_2 = 22°C	Global T if 4 × CO_2 = 25°C	Global T if 4 × CO_2 = 19°C	Global T if 4 × CO_2 = 22°C	Global T if 4 × CO_2 = 25°C
0.6835	190		0.47		0.002	0.6835	0.07	0.025	0.782	0.595	13.83	12.66	11.50	-1.17	-2.34	-3.50
1	280	1	0.70	1	0.003	1	0.11	0.21	1.313	1.000	15.00	15.00	15.00	0.00	0.00	0.00
1	280	1	0.70	2	0.006	1	0.11	0.41	1.520	1.158	16.39	17.78	19.17	1.39	2.78	4.17
1	280	1	0.70	4	0.012	1	0.11	0.83	1.935	1.473	16.77	18.53	20.30	1.77	3.53	5.30
1	280	1	0.70	8	0.024	1	0.11	1.66	2.763	2.105	17.52	20.05	22.57	2.52	5.05	7.57
1	280	1	0.70	16	0.048	1	0.11	3.32	4.421	3.367	19.04	23.08	27.11	4.04	8.08	12.11
1	280	2	1.40	1	0.003	1	0.21	0.21	1.419	1.081	16.30	17.59	18.89	1.30	2.59	3.89
1	280	2	1.40	2	0.006	1	0.21	0.41	1.626	1.238	16.49	17.97	19.46	1.49	2.97	4.46
1	280	2	1.40	4	0.012	1	0.21	0.83	2.040	1.554	16.86	18.73	20.59	1.86	3.73	5.59
1	280	2	1.40	8	0.024	1	0.21	1.66	2.869	2.185	17.62	20.24	22.86	2.62	5.24	7.86
1	280	2	1.40	16	0.048	1	0.21	3.32	4.527	3.448	19.13	23.27	27.40	4.13	8.27	12.40
1	280	4	2.80	1	0.003	1	0.42	0.21	1.630	1.242	16.49	17.98	19.47	1.49	2.98	4.47
1	278	4	2.80	2	0.006	1	0.42	0.41	1.838	1.400	16.68	18.36	20.03	1.68	3.36	5.03
1	280	4	2.80	4	0.012	1	0.42	0.83	2.252	1.715	17.06	19.11	21.17	2.06	4.11	6.17
1	280	4	2.80	8	0.024	1	0.42	1.66	3.081	2.346	17.81	20.63	23.44	2.81	5.63	8.44
1	280	4	2.80	16	0.048	1	0.42	3.32	4.738	3.609	19.33	23.66	27.98	4.33	8.66	12.98
1	280	8	5.60	1	0.003	1	0.85	0.21	2.053	1.564	16.88	18.75	20.63	1.88	3.75	5.63
1	280	8	5.60	2	0.006	1	0.85	0.41	2.261	1.722	17.06	19.13	21.19	2.06	4.13	6.19
1	280	8	5.60	4	0.012	1	0.85	0.83	2.675	2.037	17.44	19.89	22.33	2.44	4.89	7.33
1	280	8	5.60	8	0.024	1	0.85	1.66	3.504	2.669	18.20	21.40	24.60	3.20	6.40	9.60
1	280	8	5.60	16	0.048	1	0.85	3.32	5.161	3.931	19.71	24.43	29.14	4.71	9.43	14.14
1	280	16	11.20	1	0.003	1	1.69	0.21	2.900	2.208	17.65	20.30	22.94	2.65	5.30	7.94
1	280	16	11.20	2	0.006	1	1.69	0.41	3.107	2.366	17.84	20.67	23.51	2.84	5.67	8.51
1	280	16	11.20	4	0.012	1	1.69	0.83	3.521	2.682	18.22	21.43	24.65	3.22	6.43	9.65
1	280	16	11.20	8	0.024	1	1.69	1.66	4.350	3.313	18.97	22.95	26.92	3.97	7.95	11.92
1	280	16	11.20	16	0.048	1	1.69	3.32	6.008	4.575	20.49	25.97	31.46	5.49	10.97	16.46
2	560	1	0.70	1	0.003	2	0.11	0.21	2.313	1.762	17.11	19.22	21.34	2.11	4.22	6.34
2	560	1	0.70	2	0.006	2	0.11	0.41	2.520	1.919	17.30	19.60	21.90	2.30	4.60	6.90
2	560	1	0.70	4	0.012	2	0.11	0.83	2.935	2.235	17.68	20.36	23.04	2.68	5.36	8.04
2	560	1	0.70	8	0.024	2	0.11	1.66	3.763	2.866	18.44	21.87	25.31	3.44	6.87	10.31
2	560	1	0.70	16	0.048	2	0.11	3.32	5.421	4.129	19.95	24.90	29.85	4.95	9.90	14.85
2	560	2	1.40	1	0.003	2	0.21	0.21	2.419	1.842	17.21	19.42	21.63	2.21	4.42	6.63
2	560	2	1.40	2	0.006	2	0.21	0.41	2.626	2.000	17.40	19.80	22.19	2.40	4.80	7.19
2	560	2	1.40	4	0.012	2	0.21	0.83	3.040	2.316	17.78	20.55	23.33	2.78	5.55	8.33
2	560	2	1.40	8	0.024	2	0.21	1.66	3.869	2.947	18.53	22.07	25.60	3.53	7.07	10.60
2	560	2	1.40	16	0.048	2	0.21	3.32	5.527	4.209	20.05	25.10	30.14	5.05	10.10	15.14
2	560	4	2.80	1	0.003	2	0.42	0.21	2.630	2.003	17.40	19.80	22.21	2.40	4.80	7.21
2	560	4	2.80	2	0.006	2	0.42	0.41	2.838	2.161	17.59	20.18	22.77	2.59	5.18	7.77
2	560	4	2.80	4	0.012	2	0.42	0.83	3.252	2.477	17.97	20.94	23.91	2.97	5.94	8.91
2	560	4	2.80	8	0.024	2	0.42	1.66	4.081	3.108	18.73	22.45	26.18	3.73	7.45	11.18
2	560	4	2.80	16	0.048	2	0.42	3.32	5.738	4.370	20.24	25.48	30.72	5.24	10.48	15.72
2	560	8	5.60	1	0.003	2	0.85	0.21	3.053	2.326	17.79	20.58	23.37	2.79	5.58	8.37
2	560	8	5.60	2	0.006	2	0.85	0.41	3.261	2.483	17.98	20.96	23.93	2.98	5.96	8.93
2	560	8	5.60	4	0.012	2	0.85	0.83	3.675	2.799	18.36	21.71	25.07	3.36	6.71	10.07
2	560	8	5.60	8	0.024	2	0.85	1.66	4.504	3.430	19.11	23.23	27.34	4.11	8.23	12.34
2	560	8	5.60	16	0.048	2	0.85	3.32	6.161	4.693	20.63	26.25	31.88	5.63	11.25	16.88
2	560	16	11.20	1	0.003	2	1.69	0.21	3.900	2.970	18.56	22.12	25.68	3.56	7.12	10.68
2	560	16	11.20	2	0.006	2	1.69	0.41	4.107	3.128	18.75	22.50	26.25	3.75	7.50	11.25
2	560	16	11.20	4	0.012	2	1.69	0.83	4.521	3.443	19.13	23.26	27.39	4.13	8.26	12.39
2	560	16	11.20	8	0.024	2	1.69	1.66	5.350	4.075	19.89	24.77	29.66	4.89	9.77	14.66
2	560	16	11.20	16	0.048	2	1.69	3.32	7.008	5.337	21.40	27.80	34.20	6.40	12.80	19.20
4	1120	1	0.70	1	0.003	4	0.11	0.21	4.313	3.285	18.94	22.88	26.82	3.94	7.88	11.82
4	1120	1	0.70	2	0.006	4	0.11	0.41	4.520	3.443	19.13	23.26	27.38	4.13	8.26	12.38
4	1120	1	0.70	4	0.012	4	0.11	0.83	4.935	3.758	19.51	24.01	28.52	4.51	9.01	13.52
4	1120	1	0.70	8	0.024	4	0.11	1.66	5.763	4.389	20.26	25.53	30.79	5.26	10.53	15.79
4	1120	1	0.70	16	0.048	4	0.11	3.32	7.421	5.652	21.78	28.55	35.33	6.78	13.55	20.33
4	1120	2	1.40	1	0.003	4	0.21	0.21	4.419	3.365	19.04	23.07	27.11	4.04	8.07	12.11
4	1120	2	1.40	2	0.006	4	0.21	0.41	4.626	3.523	19.22	23.45	27.67	4.22	8.45	12.67
4	1120	2	1.40	4	0.012	4	0.21	0.83	5.040	3.839	19.60	24.21	28.81	4.60	9.21	13.81
4	1120	2	1.40	8	0.024	4	0.21	1.66	5.869	4.470	20.36	25.72	31.08	5.36	10.72	16.08
4	1120	2	1.40	16	0.048	4	0.21	3.32	7.527	5.733	21.87	28.75	35.62	6.87	13.75	20.62
4	1120	4	2.80	1	0.003	4	0.42	0.21	4.630	3.527	19.23	23.46	27.69	4.23	8.46	12.69
4	1120	4	2.80	2	0.006	4	0.42	0.41	4.838	3.684	19.42	23.84	28.25	4.42	8.84	13.25
4	1120	4	2.80	4	0.012	4	0.42	0.83	5.252	4.000	19.80	24.59	29.39	4.80	9.59	14.39
4	1120	4	2.80	8	0.024	4	0.42	1.66	6.081	4.631	20.55	26.11	31.66	5.55	11.11	16.66
4	1120	4	2.80	16	0.048	4	0.42	3.32	7.738	5.894	22.07	29.13	36.20	7.07	14.13	21.20
4	1120	8	5.60	1	0.003	4	0.85	0.21	5.053	3.849	19.62	24.23	28.85	4.62	9.23	13.85
4	1120	8	5.60	2	0.006	4	0.85	0.41	5.261	4.007	19.80	24.61	29.41	4.80	9.61	14.41
4	1120	8	5.60	4	0.012	4	0.85	0.83	5.675	4.322	20.18	25.37	30.55	5.18	10.37	15.55
4	1120	8	5.60	8	0.024	4	0.85	1.66	6.504	4.953	20.94	26.88	32.82	5.94	11.88	17.82
4	1120	8	5.60	16	0.048	4	0.85	3.32	8.161	6.216	22.45	29.91	37.36	7.45	14.91	22.36
4	1120	16	11.20	1	0.003	4	1.69	0.21	5.900	4.493	20.39	25.78	31.16	5.39	10.78	16.16
4	1120	16	11.20	2	0.006	4	1.69	0.41	6.107	4.651	20.58	26.15	31.73	5.58	11.15	16.73
4	1120	16	11.20	4	0.012	4	1.69	0.83	6.521	4.967	20.96	26.91	32.87	5.96	11.91	17.87
4	1120	16	11.20	8	0.024	4	1.69	1.66	7.350	5.598	21.71	28.43	35.14	6.71	13.43	20.14
4	1120	16	11.20	16	0.048	4	1.69	3.32	9.008	6.860	23.23	31.45	39.68	8.23	16.45	24.68

Table 2 (continued)

8	2240	1	0.70	1	0.003	8	0.11	0.21	8.313	6.331	22.59	30.18	37.78	7.59	15.18	22.78
8	2240	1	0.70	2	0.006	8	0.11	0.41	8.520	6.489	22.78	30.56	38.34	7.78	15.56	23.34
8	2240	1	0.70	4	0.012	8	0.11	0.83	8.935	6.805	23.16	31.32	39.48	8.16	16.32	24.48
8	2240	1	0.70	8	0.024	8	0.11	1.66	9.763	7.436	23.92	32.83	41.75	8.92	17.83	26.75
8	2240	1	0.70	16	0.048	8	0.11	3.32	11.421	8.698	25.43	35.86	46.29	10.43	20.86	31.29
8	2240	2	1.40	1	0.003	8	0.21	0.21	8.419	6.412	22.69	30.38	38.07	7.69	15.38	23.07
8	2240	2	1.40	2	0.006	8	0.21	0.41	8.626	6.570	22.88	30.76	38.63	7.88	15.76	23.63
8	2240	2	1.40	4	0.012	8	0.21	0.83	9.040	6.885	23.26	31.51	39.77	8.26	16.51	24.77
8	2240	2	1.40	8	0.024	8	0.21	1.66	9.869	7.517	24.01	33.03	42.04	9.01	18.03	27.04
8	2240	2	1.40	16	0.048	8	0.21	3.32	11.527	8.779	25.53	36.05	46.58	10.53	21.05	31.58
8	2240	4	2.80	1	0.003	8	0.42	0.21	8.630	6.573	22.88	30.76	38.65	7.88	15.76	23.65
8	2240	4	2.80	2	0.006	8	0.42	0.41	8.838	6.731	23.07	31.14	39.21	8.07	16.14	24.21
8	2240	4	2.80	4	0.012	8	0.42	0.83	9.252	7.046	23.45	31.90	40.35	8.45	16.90	25.35
8	2240	4	2.80	8	0.024	8	0.42	1.66	10.081	7.678	24.21	33.41	42.62	9.21	18.41	27.62
8	2240	4	2.80	16	0.048	8	0.42	3.32	11.738	8.940	25.72	36.44	47.16	10.72	21.44	32.16
8	2240	8	5.60	1	0.003	8	0.85	0.21	9.053	6.895	23.27	31.54	39.81	8.27	16.54	24.81
8	2240	8	5.60	2	0.006	8	0.85	0.41	9.261	7.053	23.46	31.92	40.37	8.46	16.92	25.37
8	2240	8	5.60	4	0.012	8	0.85	0.83	9.675	7.369	23.84	32.67	41.51	8.84	17.67	26.51
8	2240	8	5.60	8	0.024	8	0.85	1.66	10.504	8.000	24.59	34.19	43.78	9.59	19.19	28.78
8	2240	8	5.60	16	0.048	8	0.85	3.32	12.161	9.262	26.11	37.21	48.32	11.11	22.21	33.32
8	2240	16	11.20	1	0.003	16	1.69	0.21	17.900	13.633	31.35	47.69	64.04	16.35	32.69	49.04
8	2240	16	11.20	2	0.006	16	1.69	0.41	18.107	13.790	31.54	48.07	64.61	16.54	33.07	49.61
8	2240	16	11.20	4	0.012	16	1.69	0.83	18.521	14.106	31.92	48.83	65.75	16.92	33.83	50.75
8	2240	16	11.20	8	0.024	16	1.69	1.66	19.350	14.737	32.67	50.34	68.02	17.67	35.34	53.02
8	2240	16	11.20	16	0.048	16	1.69	3.32	21.008	16.000	34.19	53.37	72.56	19.19	38.37	57.56
16	4480	1	0.70	1	0.003	16	0.11	0.21	16.313	12.424	29.90	44.80	59.70	14.90	29.80	44.70
16	4480	1	0.70	2	0.006	16	0.11	0.41	16.520	12.582	30.09	45.18	60.26	15.09	30.18	45.26
16	4480	1	0.70	4	0.012	16	0.11	0.83	16.935	12.898	30.47	45.93	61.40	15.47	30.93	46.40
16	4480	1	0.70	8	0.024	16	0.11	1.66	17.763	13.529	31.22	47.45	63.67	16.22	32.45	48.67
16	4480	1	0.70	16	0.048	16	0.11	3.32	19.421	14.791	32.74	50.47	68.21	17.74	35.47	53.21
16	4480	2	1.40	1	0.003	16	0.21	0.21	16.419	12.505	30.00	44.99	59.99	15.00	29.99	44.99
16	4480	2	1.40	2	0.006	16	0.21	0.41	16.626	12.663	30.18	45.37	60.55	15.18	30.37	45.55
16	4480	2	1.40	4	0.012	16	0.21	0.83	17.040	12.978	30.56	46.13	61.69	15.56	31.13	46.69
16	4480	2	1.40	8	0.024	16	0.21	1.66	17.869	13.609	31.32	47.64	63.96	16.32	32.64	48.96
16	4480	2	1.40	16	0.048	16	0.21	3.32	19.527	14.872	32.83	50.67	68.50	17.83	35.67	53.50
16	4480	4	2.80	1	0.003	16	0.42	0.21	16.630	12.666	30.19	45.38	60.56	15.19	30.38	45.56
16	4480	4	2.80	2	0.006	16	0.42	0.41	16.838	12.824	30.38	45.76	61.13	15.38	30.76	46.13
16	4480	4	2.80	4	0.012	16	0.42	0.83	17.252	13.139	30.76	46.51	62.27	15.76	31.51	47.27
16	4480	4	2.80	8	0.024	16	0.42	1.66	18.081	13.771	31.51	48.03	64.54	16.51	33.03	49.54
16	4480	4	2.80	16	0.048	16	0.42	3.32	19.738	15.033	33.03	51.05	69.08	18.03	36.05	54.08
16	4480	8	5.60	1	0.003	16	0.85	0.21	17.053	12.988	30.57	46.15	61.72	15.57	31.15	46.72
16	4480	8	5.60	2	0.006	16	0.85	0.41	17.261	13.146	30.76	46.53	62.29	15.76	31.53	47.29
16	4480	8	5.60	4	0.012	16	0.85	0.83	17.675	13.462	31.14	47.28	63.43	16.14	32.28	48.43
16	4480	8	5.60	8	0.024	16	0.85	1.66	18.504	14.093	31.90	48.80	65.70	16.90	33.80	50.70
16	4480	8	5.60	16	0.048	16	0.85	3.32	20.161	15.355	33.41	51.83	70.24	18.41	36.83	55.24
16	4480	16	11.20	1	0.003	16	1.69	0.21	17.900	13.633	31.35	47.69	64.04	16.35	32.69	49.04
16	4480	16	11.20	2	0.006	16	1.69	0.41	18.107	13.790	31.54	48.07	64.61	16.54	33.07	49.61
16	4480	16	11.20	4	0.012	16	1.69	0.83	18.521	14.106	31.92	48.83	65.75	16.92	33.83	50.75
16	4480	16	11.20	8	0.024	16	1.69	1.66	19.350	14.737	32.67	50.34	68.02	17.67	35.34	53.02
16	4480	16	11.20	16	0.048	16	1.69	3.32	21.008	16.000	34.19	53.37	72.56	19.19	38.37	57.56

Climatic Interpretation after Kidder and Worsley (2002)

The first row is for the Last Glacial Maximum, with gas concentrations based on ice core data. For detailed discussion of the sources and lifetimes each of these greenhouse gases, see the relevant chapters in Hay (2016) Experimenting on a Small Planet (2nd edition)

Water on land

Most climate models have assumed that the amount of water on land in the past was analogous to today. The possibility exists that 'wet areas' such as bogs and swamps may have been much more extensive during times when the continents had lower relief overall and river gradients were much flatter was not taken into account.

Water on land—today

The modern Earth is not a good model for understanding its past conditions. The planet has just emerged from a glacial maximum with much lower sea levels and a colder climate into a warm interglacial. Many modern lakes are of glacial origin, rivers and shorelines are still adjusting to the higher sea level, and many areas are still responding to the change

in climate. In addition, human activities have greatly modified much of the Earth's surface. Topographic relief is at one of its Phanerozoic maxima, so that river courses are unusually steep. Large areas of the land surface and many rivers have been extensively altered to suit human needs. Many of these alterations occurred before river flows and sediment discharges were measured (Hay 1998). These changes of the natural environment are so extreme that the term Anthropocene has been proposed to refer to the age of human modification of the Earth (Waters et al. 2016).

Furthermore, mass balance studies (Ronov 1993; Hay 1994) indicate that Earth's modern topographic relief may be at the second of its Phanerozoic maxima. Conditions on the lower, warmer Earth of the Cretaceous may represent the other extreme condition of the planet and were very different.

The following discussion is based on the consideration of general principles deduced from analysis of modern and pre-Anthropogenic conditions and theoretical considerations.

Today the largest open water surfaces on land are lakes, rivers, and wetlands.

Lakes

A lake is a body of water surrounded by land and not connected to the sea. The total number of lakes on land today is ~ 117 million, estimated by Verpoorter et al. (2014) to have a combined surface area of about 5×10^6 km^2, about 3.7% of the Earth's nonglaciated land area.

Types of lakes commonly recognized are: (1) Tectonic lakes, such as the African Rift Valley lakes (Tanganyika, Malawi, etc.) or intra-continental subsiding basins surrounded by tectonic rises or uplifts, such as Lake Balaton in Europe, the Hoh Xil of the Tibetan Plateau, the Aral Sea, and the Great Salt Lake of North America, (2) Glacial lakes (such as the Great Lakes of North America or the perialpine lakes of Europe, (3) Crater lakes in non-active volcanic craters, (4) Lakes formed by landslides or ice dams, which are usually short-lived, (5) Sinkhole lakes, which are sinkholes that formed during lowstands of sea level during the last and earlier glacial maxima and are now filled with water, and (6) oxbow lakes, which are cut-off, isolated former river meanders. Downing et al. (2006) estimate that natural lakes and ponds cover about

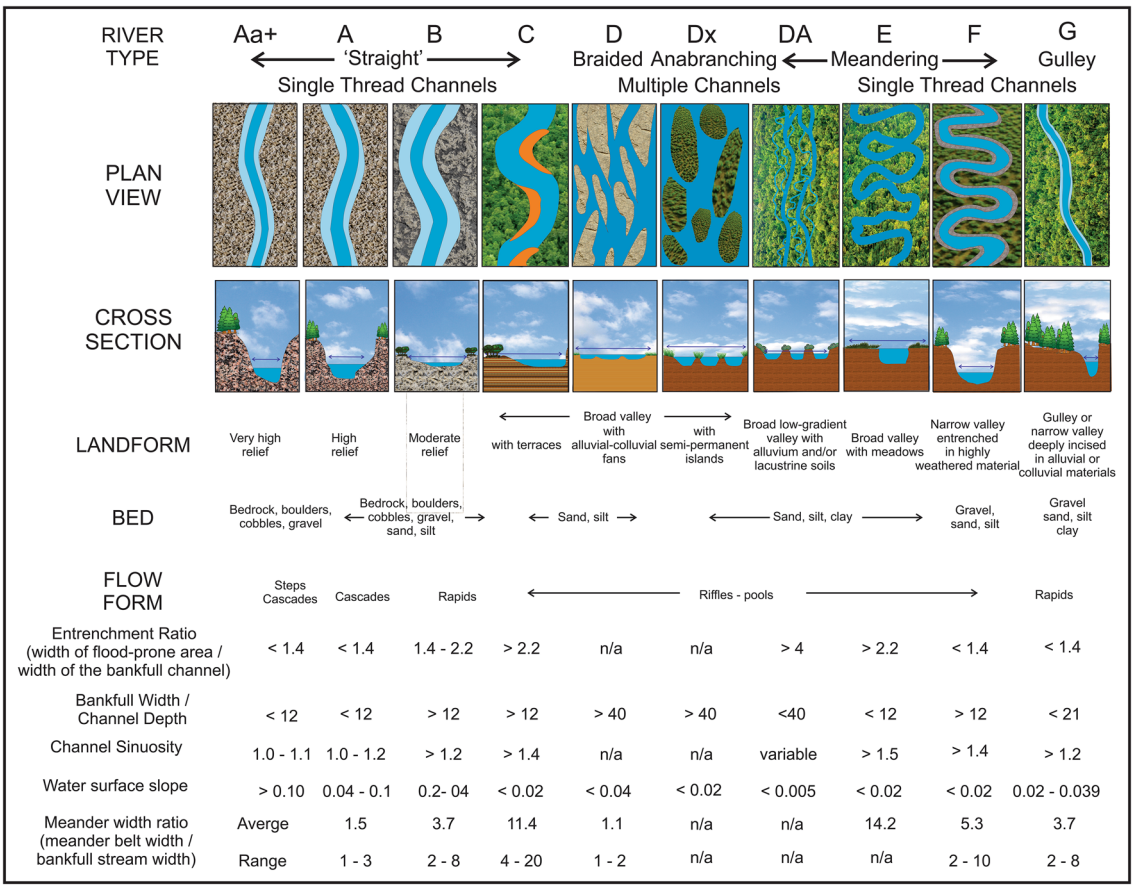

Entrenchment Ratio (width of flood-prone area / width of the bankfull channel)	< 1.4	< 1.4	1.4 - 2.2	> 2.2	n/a	n/a	> 4	> 2.2	< 1.4	< 1.4
Bankfull Width / Channel Depth	< 12	< 12	> 12	> 12	> 40	> 40	<40	< 12	> 12	< 21
Channel Sinuosity	1.0 - 1.1	1.0 - 1.2	> 1.2	> 1.4	n/a	n/a	variable	> 1.5	> 1.4	> 1.2
Water surface slope	> 0.10	0.04 - 0.1	0.2- 04	< 0.02	< 0.04	< 0.02	< 0.005	< 0.02	< 0.02	0.02 - 0.039
Meander width ratio (meander belt width / bankfull stream width)	Averge	1.5	3.7	11.4	1.1	n/a	n/a	14.2	5.3	3.7
	Range	1 - 3	2 - 8	4 - 20	1 - 2	n/a	n/a	n/a	2 - 10	2 - 8

Fig. 7 River types discussed in text and their characteristics, after Rosgen, (1994) and other sources

4.2 million km^2 of the earth's surface, but this might not include all of the many small lakes of the circum-Arctic region. Reservoirs, artificial lakes produced by damming rivers, have an area of about 0.28 million km^2 (total from Wikipedia List of reservoirs by surface area).

Tectonic lakes, like those of the eastern African Rift and Lake Baikal in central Asia are long, narrow and deep. They have steep sides, with very restricted shallow water areas. They are the second largest group of lakes in existence today. Cretaceous examples would include the long-lived lake in the Songliao Basin (Song et al. 2014, 2015), other lakes in eastern Asia, the rift valley lakes formed as South America separated from Africa, and other areas undergoing rifting (Hay 1981).

Glacial lakes are the largest lakes in existence today. The Great Lakes of North America are located along the boundary of the hard rocks of the Precambrian Canadian Shield and the softer Paleozoic sedimentary rocks surrounding it. Much of northern North America, Europe and Asia is covered by innumerable small lakes in depressions between moraines. None of these features existed during the Cretaceous. The proposition that there were glaciers during the warm middle Cretaceous (Miller et al. 2003) was based on misinterpretation of the $\delta^{18}O$ record of oceanic calcareous fossils (Wendler and Wendler 2016). There may have been some small glacial lakes in the Early Cretaceous in the Eromanga region of southeastern Australia, evidenced by dropstones in sediments near the Livingston Tillite (Alley and Frakes 2003).

Lakes may occur in volcanic craters or meteorite–asteroid impact structures, but these are generally small and, in any case, rare. Perhaps the largest today is Yellowstone Lake in the huge Yellowstone caldera. There were undoubtedly some crater lakes present from time-to-time during the Cretaceous which may have had minor local effects, but they would not have had any regional or global effects.

With the low topographic relief, lakes formed by landslides would have been very rare and short-lived. There was no possibility of significant ice dammed lakes.

Modern sinkhole lakes are related to the rapidly changing sea levels associated with the Quaternary glaciations and interglacials. They are too small to have any climatic effects. Because of the widespread occurrence of limestone deposits and slower sea-level fluctuations during the Cretaceous, similar features might have existed then and may even have been much more widespread.

In contrast to all the other kinds of lakes, oxbow lakes, discussed at greater length below, were probably very abundant. Oxbow lakes are isolated cutoff river meanders. They have many of the same features as a meandering river, a width many times their depth, a depth of typically 4–8 (certainly more than 2 and less than 10) m, a relatively hard bottom of coarser sediment, and muddy bank margins.

Rivers

Rivers are the major way in which runoff is delivered to the ocean. Today the water surface area of rivers is estimated to be between 485,000 and 662,000 km^2 or 0.36–0.49% of the nonglaciated land area (Downing et al. 2012). Recent studies using satellite imagery indicate that these estimates are low and that the true area is of the order of twice as large. (https://earthobservatory.nasa.gov/images/92432/the-water-is-wider).

Classically, there are three types of river courses: straight, braided, and meandering (Leopold and Wolman 1957). There are many factors which induce the instabilities that determine whether a river will be braided or meandering, including slope, flow rate, turbulence, bed transport load, suspended load (Callander 1969, 1978; Fredsøe 1978; Schumm 1985; Constantine et al. 2010; Davies et al. 2011).

The velocity of water in a river varies with slope (Leopold 1953) and depth, with highest velocities at the surface decreasing sharply near the bed and sides, Friction with the sides causes the water to form eddies; typically, these erode the bank on one side of the river and deposit material on the other side, leading to a sinuous and eventually meandering river course.

Straight rivers (Aa+, A, B, and C in Fig. 7) are characteristic of a relatively steep downhill course with uneven bottoms. The straight segment is rarely more than ten times the width of the channel (Leopold and Wolman 1957).

A 'braided river' (D in Fig. 7) has many small channels separated by small ephemeral bars or islands Braiding is typical of river segments having a steep slope and/or large sediment load. Braiding also occurs in environments such as alluvial fans and river deltas that dramatically decrease channel depth and flow velocity. There the braids are referred to as distributaries. To these an older category, used originally to describe some Australian rivers, has recently been revived: anabranching (Latrubesse 2008).

The term 'ana-branch' was proposed by Jackson (1834) to describe some rivers in Australia. An 'anabranching river' (Dx in Fig. 7) has two or more main channels separated by semi-permanent islands. It has been subsequently recognized that this is a feature common to many large lowland rivers, especially those crossing through dry areas. Of the world's ten largest rivers, only one, the Mississippi, is not anabranching. Another type of fluvial system, resembling but not synonymous with anabranching rivers, are anastomosing rivers. An anastomosing river is composed of two or more interconnected channels that enclose flood basins and is formed under relatively low-energy conditions near the local base level (Makaske 2001). Given the low continental relief during the Mid-Cretaceous, anastomosing river systems may have occurred more frequently than today.

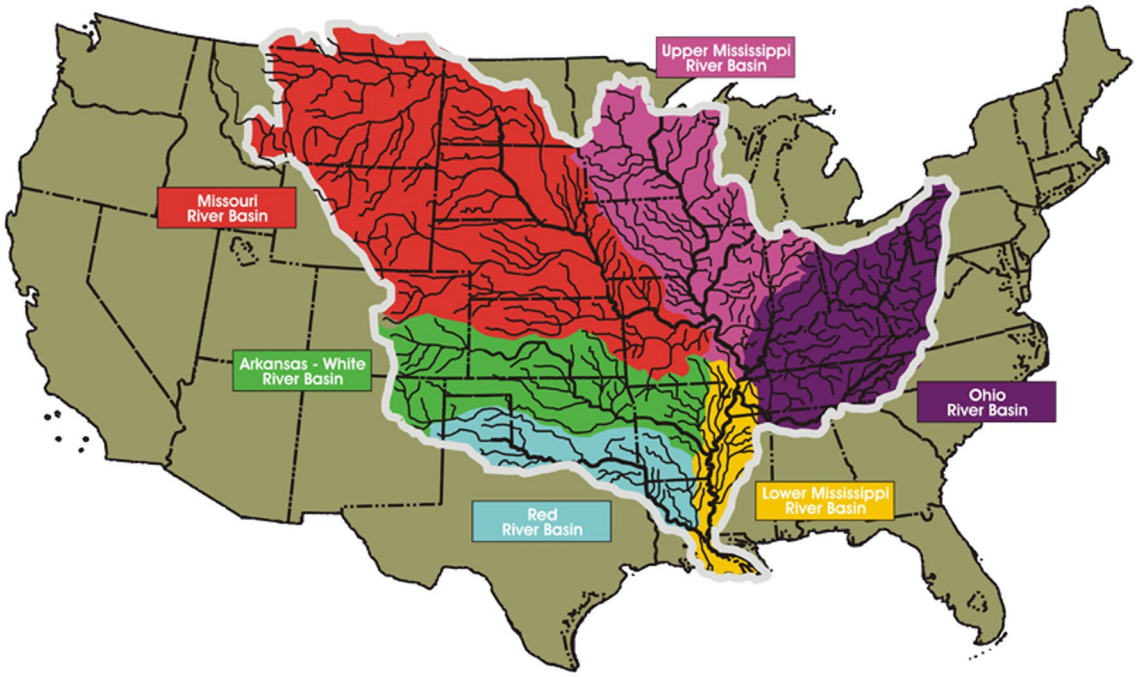

Fig. 8 The Mississippi River watershed, showing its major drainage basins. Map courtesy of the Mississippi River Commission

A 'meandering river' (DA, E, and F in Fig. 7) is a watercourse with a migrating sinuous path (Leopold and Wolman 1960; Stølum 1998). Meandering is induced by a low slope and/or large suspended sediment load. The maximum flow velocity alternates from one side of the channel to the other, so that the material eroded from the bank on the outer part of the curved channel is then deposited on the same side of the river, on the inner part of the subsequent curve, often as a 'point bar'. As the river channel migrates, the meander may have a small neck which is ultimately cut through, leaving the older meander isolated as an oxbow lake.

A 'gulley' (G in Fig. 7) is a trench or small valley carved by running water during major rainstorms.

As a river approaches the coast its slope approaches zero and it may divide into a series of distributary channels, as mentioned above. For the Mississippi and Ganges–Brahmaputra system, this occurs about 200 km inland; for the Amazon, the distributary system starts about 250 km inland.

The Mississippi River, although undoubtedly much larger than those of the Cretaceous, may give insights into what ancient lowland river systems may have been like. Although the Mississippi River's drainage basin is large (2,981,076 km^2, almost 1/3 of the area of North America) it is smaller than those of the Amazon and Congo. It is the best known but has been extensively modified over the past few centuries. Its average discharge rate, measured at Vicksburg, Mississippi over the past 200 years is about 18,000 m^3/s (Turner and Rabalais 2003). The river's source is considered to be Lake Itasca, Minnesota, in a basin formed during the last glaciation, with an elevation of 450 m. Lake Itasca itself is fed by several small streams. The Mississippi River has a length of 3734 km. Its major tributaries include the Missouri River (nicknamed The Big Muddy) from the west, the Ohio River from the east, and the Arkansas and Red Rivers from the west. The Missouri River's primary source has an elevation of 2774 m; it is the longest in North America, 3767 km from its source to its junction with the Mississippi near St. Louis, Missouri (elevation 123 m). Its average slope is 0.0007/1 m (70 cm/km). Both its upper reaches and its tributaries are mostly straight or braided, but the lower half was meandering before the construction of dams. The Ohio River's primary source is in the Allegheny Mountains of Pennsylvania at an elevation of 683 m; its length is 1579 km before it joins the Mississippi near Cairo, Illinois (elevation 88 m). Both it and its tributaries are mostly straight or braided except for its lowest section which has large meanders. Its average slope is 0.00038/1 (38 cm/km). The stretch of the river from Cairo to the Gulf of Mexico is called the Lower Mississippi. Its width (measured using Google Earth) generally ranges between 1 and 1.5 km; its depth above Baton Rouge is about 3 m, and its slope is about 0.00006/1 (6 cm/km). Its width to depth ratio is > 400. A lower tributary, the Arkansas River, has its primary source is near Leadville, Colorado, at an elevation of 2965 m; its length is 2364 km to its junction with the Mississippi near Napoleon, Arkansas (elevation 33 m). Its average slope is 0.00124/1. The upper reaches of the river are straight or braided, but below Ponce City, Oklahoma,

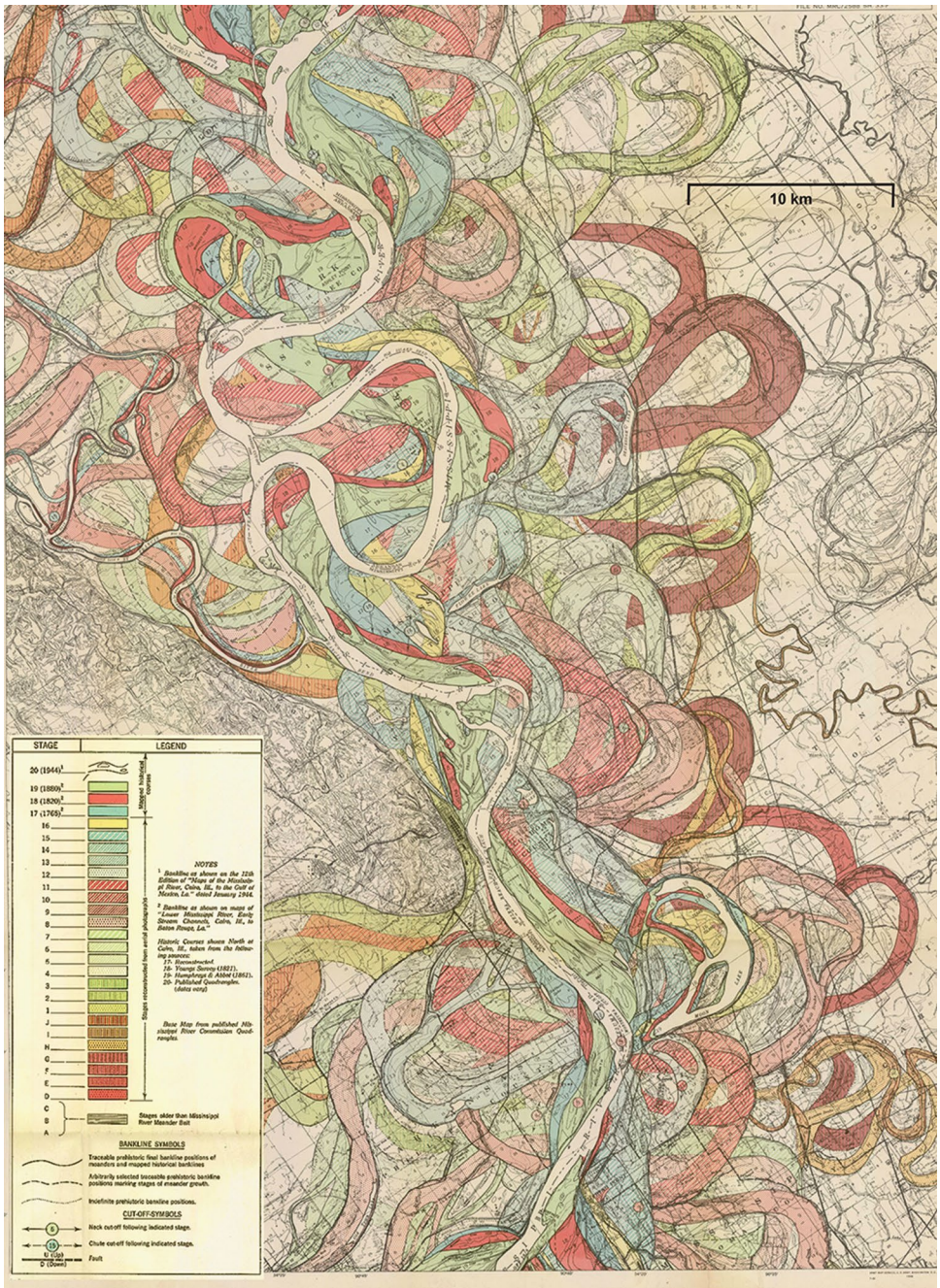

Fig. 9 The Mississippi River meander belt from 34°55′ to 34°30′ (Arkansas–Tennessee) analyzed from aerial photographs. 26 older meander traces (former or existing oxbow lakes) are shown. From Fisk (1944) Plate 22-6

it meanders. Although it has tributaries extending into the Texas panhandle, the Red River's (Red River of the South) primary source is officially in Harmon County, Oklahoma, at an elevation of 468 m; its length is 2190 km to its junction with the Lower Mississippi/Atchafalaya complex near Alexandria, Louisiana (elevation 9.1 m). Its average slope is 0.00021/1. Most of the Red River course is meandering. The Atchafalaya River is a distributary of the Mississippi originating where the Red River joins the Mississippi and flows generally parallel to and west of the main channel. Its mouth into the Gulf of Mexico is at Atchafalaya Bay, west of the main Mississippi delta.

Below Baton Rouge the channel deepens, from about 13 to 60 m as it passes through New Orleans. This deep channel is left over from the Last Glacial maximum, when sea level in that region was about − 130 m. Today a channel depth of 45 ft (13.6 m) to Baton Rouge is maintained by dredging to allow passage of large ships (Figs. 8, 9).

The Mississippi River changes from a more or less straight or braided river to a meandering river after its junction with the Ohio River near Cairo, Illinois. From there to

the Gulf of Mexico it is referred to as the Lower Mississippi and its course is meandering. The straight-line distance from Cairo to the mouth of the Mississippi River is about 800 km. The elevation difference is 96 m. The straight-line slope is then 96/800,000, or 0.00012 m/m. However, because of its meandering course, the distance along the river channel from Cairo to the mouth of the Mississippi River is presently about 1600 km, so that the slope is 0.00006 m/m. However, this is the modern river length, and since the early 1900's many meanders have been cut through, so that the original river length from Cairo to the mouth may have been about 2400 km, for a slope of 0.00004 m/m.

The Lower Mississippi's first distributary on approaching the coast is the Atchafalaya River, which originates near Simmesport, Louisiana, where the Red River joins the Mississippi system, at an elevation of 9.1 m. It is 220 km long; its slope is 0.000041/1.

A series of detailed maps of the Mississippi River from Cape Girardeau, Missouri (about 45 km north of the confluence with the Ohio River) to its mouth into the Gulf of Mexico was prepared by Harland Fisk and published in 1944, before many of the modifications of the river were made. These maps, based on aerial photographs, show not only the river course, but three historic and 25 older Quaternary abandoned meander courses. Many of these would have been (or are) oxbow lakes. These maps give an idea of the original extent of water covered areas associated with the river. However, their lateral extent may be limited by the overall width of the Mississippi valley which was formed during Quaternary sea-level lowstands.

At its source from Lake Itaska, the Mississippi River is less than 1 m deep; its average flow rate is about 0.17 m/s; the surface velocity of the water is about 0.53 m/s. At New Orleans the flow rate is 100,000 times greater and the velocity at the surface of the water is about 1.33 m/s. The depth of the river changes dramatically with the season: at Memphis, TN; the depth during the dry season is less than 3 m, but at high water in late spring it averages about 12 m.

Oxbow lakes in the Lower Mississippi valley are short-lived ($\pm$100 year) because they are rapidly filled in by the river's muddy spring floods related to snow-melt in the Great Plains and Rocky Mountains.

Wetlands

Wetlands are areas saturated with water, such as swamps, marshes, bogs, and fens. Swamps are dominated by woody plants and are forested; marshes are dominated by herbaceous vegetation; bogs are wetlands with acidic water that accumulate peat, the vegetation is often dominated by mosses; fens are wetlands with neutral or alkaline waters usually dominated by grasses, sedges, and brown mosses. Their present areal extent of wetlands is more difficult to determine but is estimated to be between 4.8 and 12.9×10^6 km^2 or between 3.6 and 9.6% of the nonglaciated land area (Melton et al. 2013), almost equal to or perhaps even twice as much as the combined areas of lakes and rivers. However, it is known that the area of wetlands has been greatly reduced, perhaps by as much as one-half, by human activities associated with the rise of civilization over the past millennia.

The total area of water surfaces existing on land today is probably between 10.5 and 18.5×10^6 km^2, or between about 8 and 14% of the nonglaciated land area. It is reasonable to assume that prior to human modification of the landscape; these values might have been about twice what they are today.

Total global precipitation in the latter part of the last century has been reported as 573×10^{12} m^3 (Legates and Willmott 1990), but again, this value is probably too low as an estimate for precipitation prior to modification of the landscape by human activities.

Groundwater

A significant flow of water from land to sea occurs as groundwater directly entering the ocean (Rodellas et al. 2015). Because this does not interact directly with the climate system it is not included in climate models.

Water on land in the Cretaceous

The distribution of water on land during the Mid-Cretaceous was very different from that today. We estimate that the total land area at that time was about 80% of the present land area: 148.5×10^6 km$^2 \times 0.8 = 118.8$ km^2. The major landmasses were Western North America, Eastern North America, Eurasia, South America, Africa, India, and Antarctica-Australia. The separation between Eastern North America and Eurasia was a rift-valley seaway too narrow to be shown on the map used for the climate model simulations (Fig. 5). The land areas were more evenly distributed between the northern and southern hemispheres. The distances between continental interior and the ocean were at their Phanerozoic minimum. This means that it was easier for water vapor that entered the atmosphere from the ocean to fall out as precipitation over land.

Precipitation rates over land were higher than today, but evaporation rates were also higher. Because of the reduced seasonality, precipitation rates would have been more constant over the year. Soil moisture levels and runoff would have been more constant throughout the year. Infiltration into the groundwater system would have been about the same as today, but with higher precipitation rates this

means greater runoff. The infiltrated groundwater returns, with a time lag usually of the order of tens to hundreds of years, as springs feeding into the rivers or diluting coastal waters (Flögel et al. 2010).

During the Cretaceous there were some tectonic lakes, such as that in the Songliao Basin, where the lake persisted throughout almost the entire Cretaceous (Song et al. 2014) along with other smaller basins of northeastern and southern Asia. There were a series of narrow rift valley lakes that formed between South America and Africa as the continent separated. These had a history like that of the modern Galilee-Dead Sea system, described in Hay (1981). During their fresh-water lake phase they accumulated large amounts of organic carbon which are now being exploited as petroleum. Similar lakes must have existed between Africa and Antarctica-India-Australia as Gondwana broke apart. Rift valley lakes have steep sides and narrow shallow marginal areas.

Because of the very gentle seaward slope of most of the land and lack of uplifts, there were probably many small rivers and only a few large ones. Almost the entire river course would have been meandering, and oxbow lakes much more common than today. The relative surface area of rivers and their associated lakes could have well been double or triple what it is today. Because of the low relief, there would have been less suspended load in the rivers, and with less seasonal flooding the lifetime of oxbow lakes would have been much longer than today. If the flow of groundwater was the major return path of water to the ocean, reducing the importance of rivers, the occurrence of oxbow lakes and natural lakes in tectonic depressions may have been favored.

Although sea-level was at its Mesozoic maximum, with large areas of the continents becoming shelf seas, the amount of non-marine sediment deposited during the Late Jurassic and Cretaceous was larger than at any other time during the Mesozoic or Cenozoic (Ronov 1993, Table 21). This must be due to the low relief and the very gradual long-term sea level rise in combination with ongoing sediment supply.

Because of the low continental relief, much of the landscape adjacent to and between the rivers and lakes would have been swamps, marshes, bogs or fens. Although apparently covered with vegetation, these areas would have had a very large surface area of water.

Recall that modern global topographic relief is close to or at its Phanerozoic maximum whereas in the Mid-Cretaceous global topographic relief was at its minimum, as shown in Fig. 5. Typical slopes below the 100 m contour on the Turonian paleotopography were of the order of 0.00006 m/m (6 cm/km), half that of the slope between Cairo, Illinois and the mouth of the Mississippi River (and that of the Rhine in The Netherlands) or about equal that in the Ganges–Brahmaputra distributaries region between Dhaka, Bangladesh, and the coast. It is likely that except for the few highland areas, rivers over all of the Turonian land areas would have had multiple meandering channels generating many oxbow lakes as testified by the sedimentary record in many places.

The implication is that there may have been much more water on land than most climate models have assumed. This would raise temperatures over land and lessen the meridional temperature gradient (Hay 2017). The goal of this paper is to explore the consequences of wetter landscapes on Mid-Cretaceous climates, and to consider the changing habitat conditions that developed during the Mesozoic. The climate simulations discussed below use values of 25%, 50% and 75% water on land to explore their effects on climatology. As noted above, it is likely that the amount of water on land during the early Holocene may have been about 25%, so the proposed much greater water-covered areas on middle Cretaceous land are appropriate.

Numerical simulations of Mid-Cretaceous (94 ma) climate

To evaluate the effects of low topography, varying greenhouse gas concentrations, and varying extents of water cover on land, a series of numerical climate simulations were carried out using the GENESIS GCM (Alder et al. 2011; Thompson and Pollard 1997). This version of the GCM uses a slab ocean component, rather than a full-depth dynamical ocean model. The slab ocean model improves computational efficiency, simplifies the interpretation of the sensitivity tests described below, and avoids complications associated with uncertain Cretaceous bathymetric boundary conditions. The 50-m slab ocean includes prognostic sea surface temperatures, accounts for ocean heat transport as a function of the paleogeography and local temperature gradient and includes dynamic-thermodynamic sea ice. The atmospheric component of the GCM has a spectral resolution of T31 (~3.75°) with 18 vertical layers and uses an adapted version of the NCAR CCM3 radiation code (Kiehl et al. 1998). The atmosphere is coupled to 2° × 2° surface models including the slab ocean-sea ice component, a six-layer soil model, a multilayer snow model, and vegetation. The model atmosphere and surface components are linked through calculations of momentum transfer and fluxes of energy and water between the atmosphere, ocean, ice, soil, and upper and lower vegetation canopies. This version of the GCM has an equilibrium climate sensitivity to a doubling of atmospheric CO_2 of 2.9 °C (DeConto et al. 2012a, b).

GCM boundary conditions and inputs for these models include a solar constant of 1337 W/m^2 and assume a circular orbit (zero eccentricity) with an obliquity of 23.5°. Global continental geography is provided by the new, low 94 Ma topography discussed above. Following the scheme

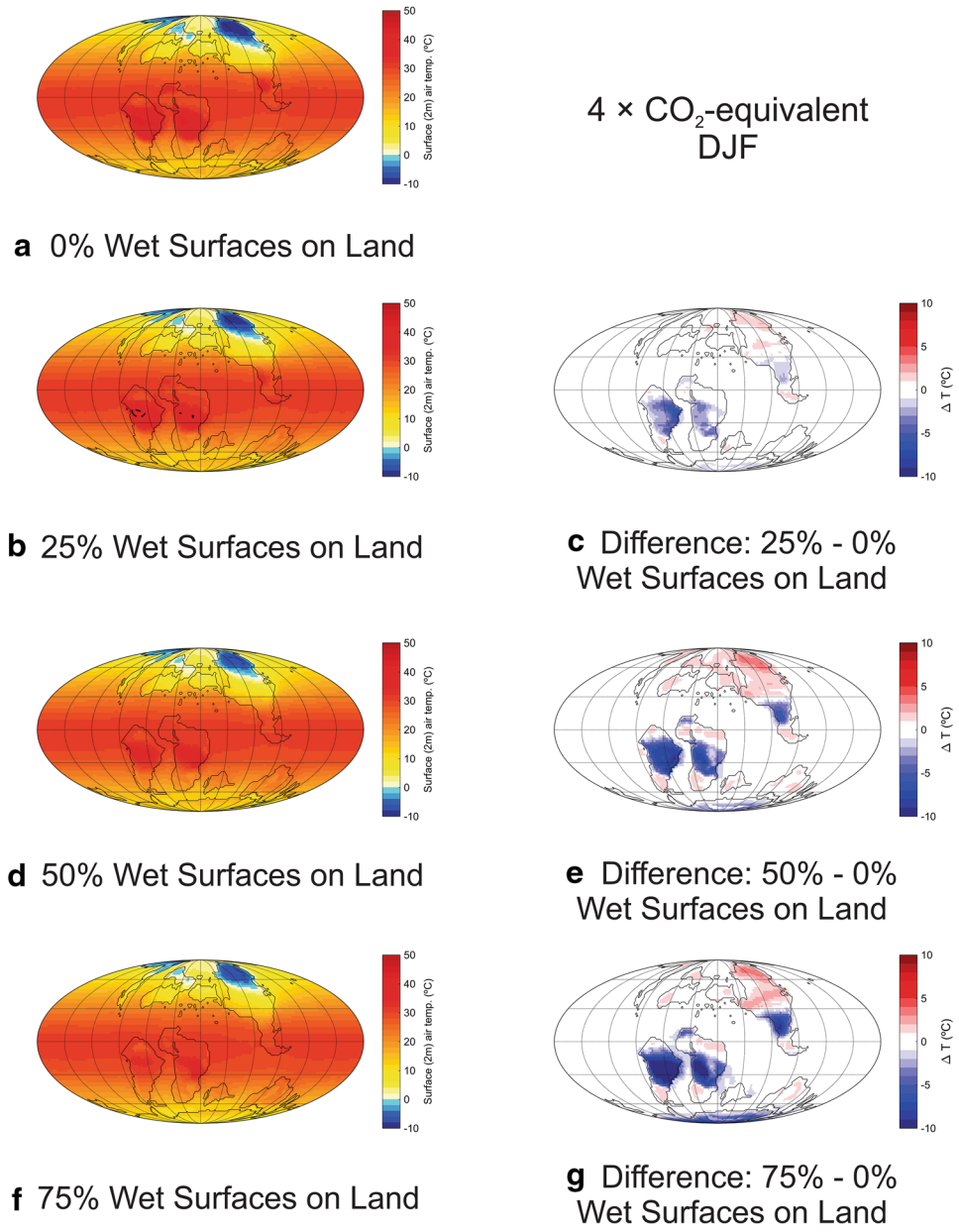

Fig. 10 Climate simulations for 4 × 'preindustrial CO_2 equivalent' (1120 ppmv) showing surface (+2 m) temperature average for Northern hemisphere winter (December–January–February) with no extensive wet surfaces on land, 25% wet surfaces on land 50% wet surfaces on land, and 75% wet surfaces on land with plots of the differences between the 25%, 50%, and 75% simulations and the 0% simulation

of DeConto et al. (2012a), the simulations were run for 4, 8, and 16 times modern 'CO_2 equivalent' greenhouse concentrations, without specifying the particular combinations of CO_2, CH_4 and N_2O. Unknown Cretaceous soil textures controlling soil hydraulic properties are defined as the fractional percentage of sand, silt, and clay in each soil layer. They are set at 51%, 29%, and 20%, respectively. These values are based on modern, global averages in ice-free latitudes (DeConto et al. 2012a, b). Land surface areas with elevations below 100 m were specified as 0%, 25%, 50%, or 75% covered by water, representing the summed areal extent of rivers, lakes, and bogs. These values represent total fractional water coverage, assumed to be distributed evenly throughout each model grid cell. The water depth is assumed to be shallow and is set at 5 m. If the water temperature falls below freezing, ice forms following the physics used in the ocean sea-ice model, except without ice advection.

Vegetation is simulated using the BIOME4 Interactive Vegetation Model of Kaplan et al. (2003), interactively coupled to the GCM. It is a coupled carbon and water

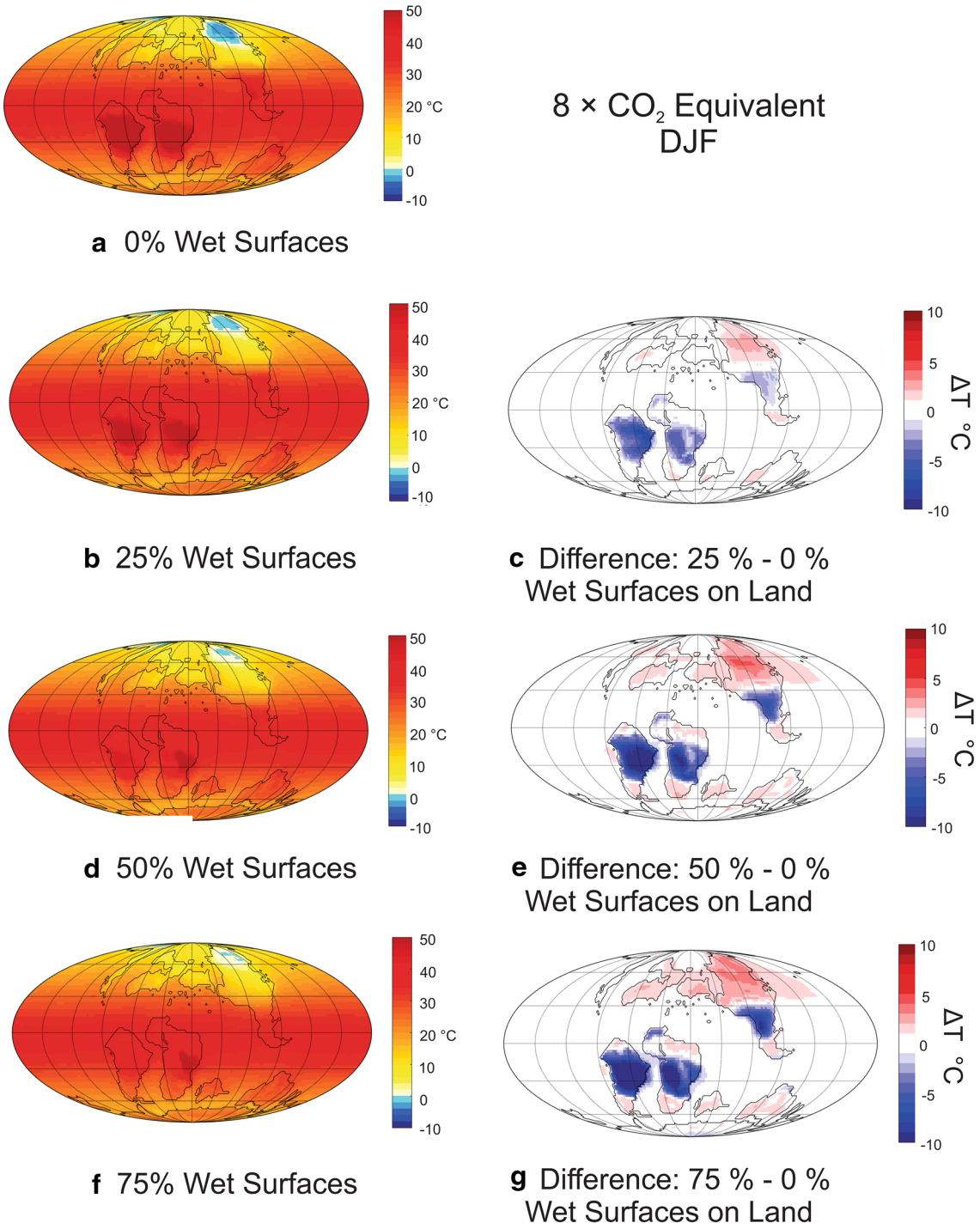

Fig. 11 Climate simulations for 8 × 'preindustrial CO_2-equivalent' (2240 ppmv) showing surface (+2 m) temperature average for Northern hemisphere winter (December–January–February) with no extensive wet surfaces on land, 25% wet surfaces on land 50% wet surfaces on land, and 75% wet surfaces on land with plots of the differences between the 25%, 50%, and 75% simulations and the 0% simulation

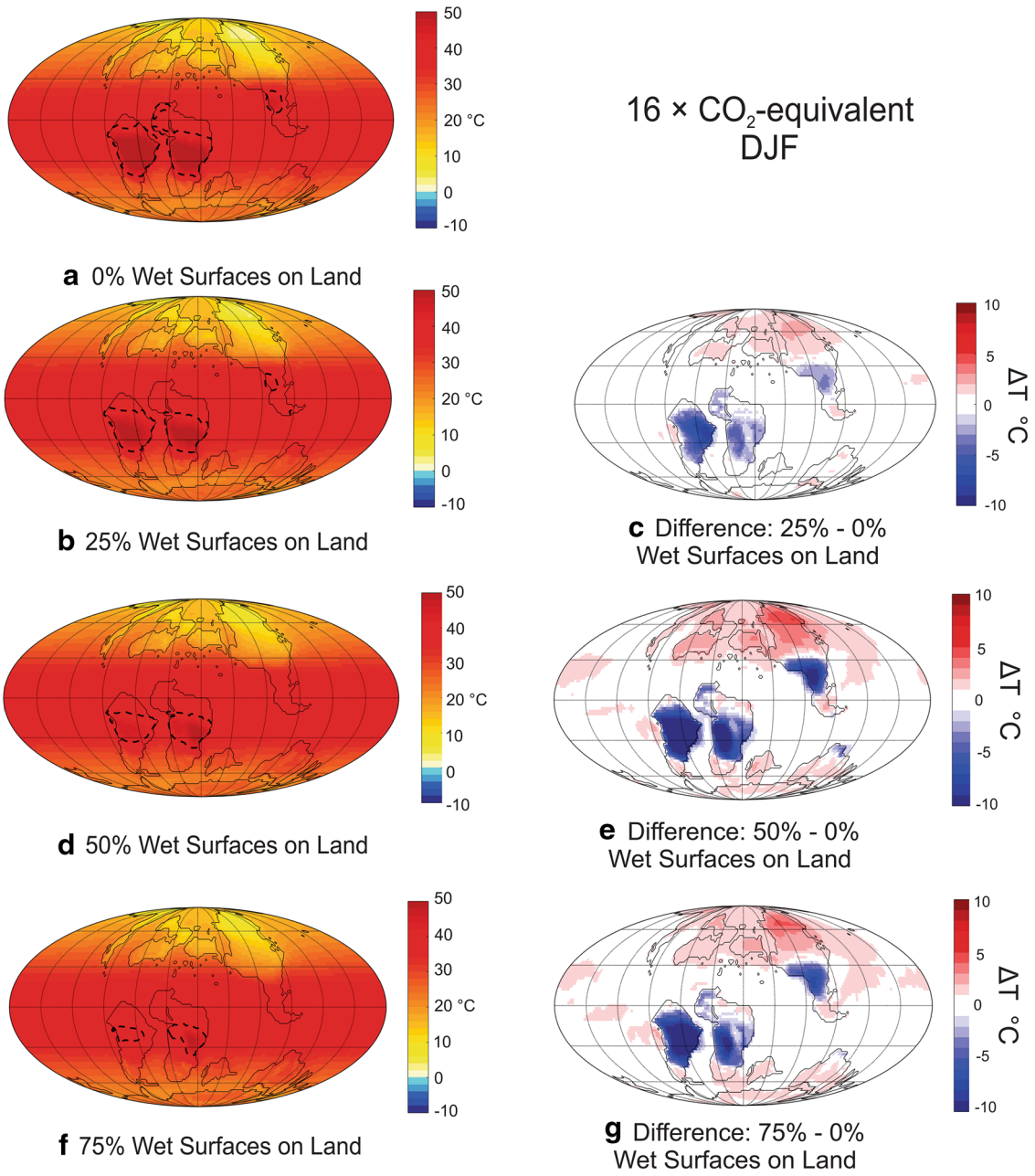

Fig. 12 Climate simulations for 16 ×'preindustrial CO_2-equivalent' (4480 ppmv) showing surface (+2 m) temperature average for Northern hemisphere winter (December–January–February) with no extensive wet surfaces on land, 25% wet surfaces on land 50% wet surfaces on land, and 75% wet surfaces on land with plots of the differences between the 25%, 50%, and 75% simulations and the 0% simulation. Photosynthetic plants, limited by RuBisCO (RUBISCO) to temperatures > ~ 32 °C would be excluded from much of Earth's surface. The 40 °C isotherm, which would outline a total exclusion zone for plants, is indicated by a heavy dashed black line. See text for discussion

flux model that simulates global steady state vegetation distribution, community structure, and biogeochemistry. The vegetation model is driven by monthly mean averages of temperature, sunshine, and precipitation provided by the GCM. In turn, the distribution of simulated vegetation affects the GCM through changes in surface roughness and energy and moisture transfer between the land surface and atmosphere. BIOME4 predicts the distribution of 27 biomes, based on 12 plant functional types (PFTs) representing broad, physiologically distinct classes ranging from cushion forbs to tropical rain forest trees (Kaplan 2001). In our Cretaceous simulations, C_4 grasses are excluded because they did not evolve until later.

The climate-vegetation simulations are run for 50 model years to ensure quasi-equilibrium. Climatological fields are calculated as monthly means, averaged over the

last 10 years of each simulation. Because virtually all of the available paleoclimate documentation from fossils and sedimentary deposits relates to limiting northern hemisphere winter temperatures, the climate simulations shown below are averages for the combined winter months of December through February (DJF).

Simulations for Northern Hemisphere winter at 94 Ma, assuming 4 × preindustrial greenhouse gas concentrations (4 × 280 ppmv = 1120 ppmv) and variable wetland areas

Figure 10a shows climate simulations for northern hemisphere winter (DJF) assuming 4 × 'preindustrial CO_2 equivalent' (280 × 4 = 1120 ppmv) atmospheric greenhouse gas concentrations. The initial simulation assumes 0% lakes and negligible river and wetland surfaces. Hence, land surface contributions to atmospheric water vapor are mainly limited to evaporation from soil surfaces and transpiration of plants. This corresponds to the standard conditions used in most numerical models of paleoclimates.

Figure 10b shows the temperature differences from Fig. 10a, based on a climate simulation using the boundary conditions described above except that 25% of the land surface, excluding the desert areas beneath the subtropical highs defined in Fig. 10a, is covered by lakes, river surfaces, and wetlands which supply additional water vapor to the atmosphere. Figure 10c shows the temperature differences from Fig. 10a but assuming that 50% of the land surface, excluding the desert areas beneath the subtropical highs defined in Fig. 10a, is covered by lakes, river surfaces, and wetlands. Figure 10d shows the temperature differences from Fig. 10a, but assuming that 75% of the land surface, is covered by lakes, river surfaces, and wetlands. Figure 10e is analogous to Fig. 10a. It shows global temperatures during northern hemisphere winter assuming that 75% of the non-desert land area is covered by lakes, river surfaces, and wetlands which supply water vapor to the atmosphere. In all of these simulations there are extensive areas of the Arctic that are below freezing and do not reflect the conditions indicated by fossils plants and reptiles as discussed above.

Simulations for Northern Hemisphere winter at 94 Ma, assuming 8 × preindustrial greenhouse gas concentrations (280 × 8 = 2240 ppmv) and variable wet areas

Figure 11 follows the format of Fig. 10, except using 8 × 'preindustrial CO_2 equivalent' (2240 ppmv) atmospheric greenhouse gas concentrations in the GCM. Importantly, the simulation assuming 8× 'CO_2 equivalent' with extensive (75%) water cover maintains above freezing Arctic temperatures during winter (Fig. 10e) reflecting the conditions indicated by fossils plants and reptiles as discussed above. Figure 11d, e still show a small region of eastern Siberia with below freezing temperatures, but these are over the upland area shown in Fig. 5. The site of the Grebenka paleoflora was at a lower elevation and would not have experienced winter temperatures below freezing.

Simulations for Northern Hemisphere winter at 94 Ma, assuming 16 × preindustrial greenhouse gas concentrations (280 × 16 = 4480 ppmv) and variable wetland areas

Figure 12 shows three climate simulations using 16 × 'preindustrial CO_2 equivalent' (280 × 16 = 4480 ppmv) with 25%, 50% and 75% lakes, river surfaces, and wetland areas. Although these simulations, like those for 4 × and 8 × CO_2 equivalent show progressive flattening of the equator to pole meridional temperature gradient, they indicate that there would be extensive areas that would be inhospitable to plant life.

The activity of an enzyme critical to photosynthesis, RuBisCO (RUBISCO—Ribulose-1,5-bisphosphate carboxylase oxygenase) is temperature limited and essentially ceases activity at temperatures above 32 °C (Jensen 2000; Crafts-Brandner and Salvucci 2000; Ellis 2010; Liu et al. 2010). In these simulations temperatures above 32 °C are widespread and essentially cover most of the land areas between 35°N and 40°S. The 40 °C isotherm, which would certainly outline an exclusion zone for plants, is shown as a heavy dashed black line in Fig. 12. The differential warming of the Arctic is less pronounced than in the 8 × CO_2 equivalent simulations.

Discussion of the climate simulations

The effect of increasing water cover can be clearly seen in Figs. 10 and 11, generally warming the northern hemisphere continental interiors in winter, and cooling the southern

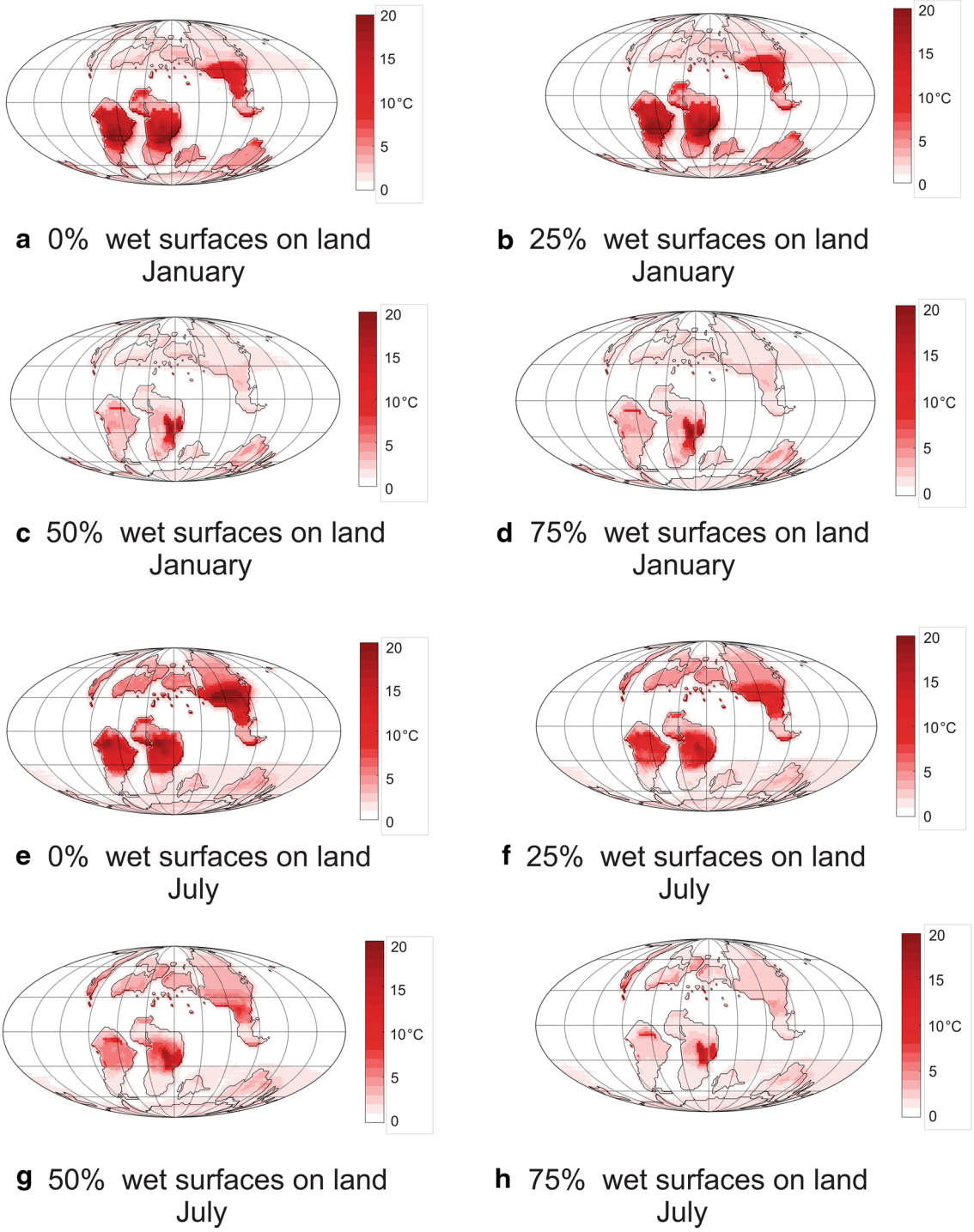

Fig. 13 Diurnal temperature ranges for January and July with 8 × preindustrial CO_2 equivalent greenhouse gas concentrations and differing areas of water surface

hemisphere continents during their respective summer. The northern hemisphere winter simulations described above define the levels of CO_2 equivalent greenhouse gases and wetland coverage on the continents required to be compatible with the paleofloras (Spicer et al. 2008; Herman and Spicer 1996, 1997, 2010) and fossil crocodilian reptiles (Tarduno et al. 1998).

None of the 4 × 'preindustrial CO_2 equivalent' simulations adequately warm the Arctic region, indicating

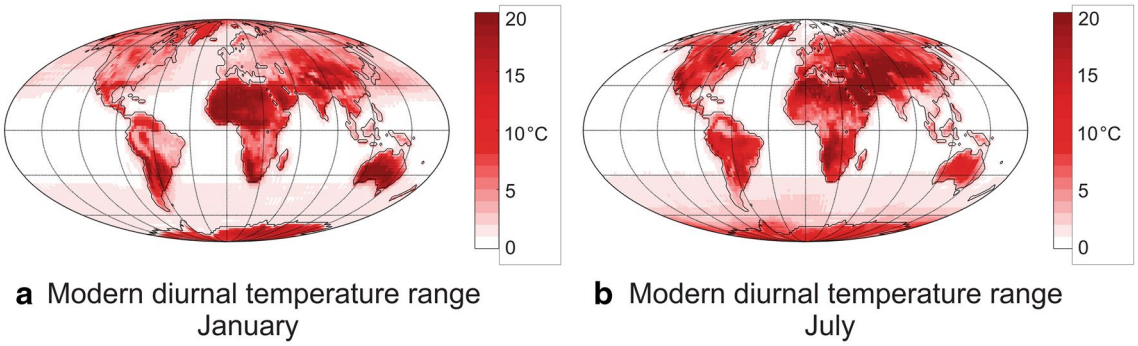

Fig. 14 Modern diurnal temperature ranges for January and July

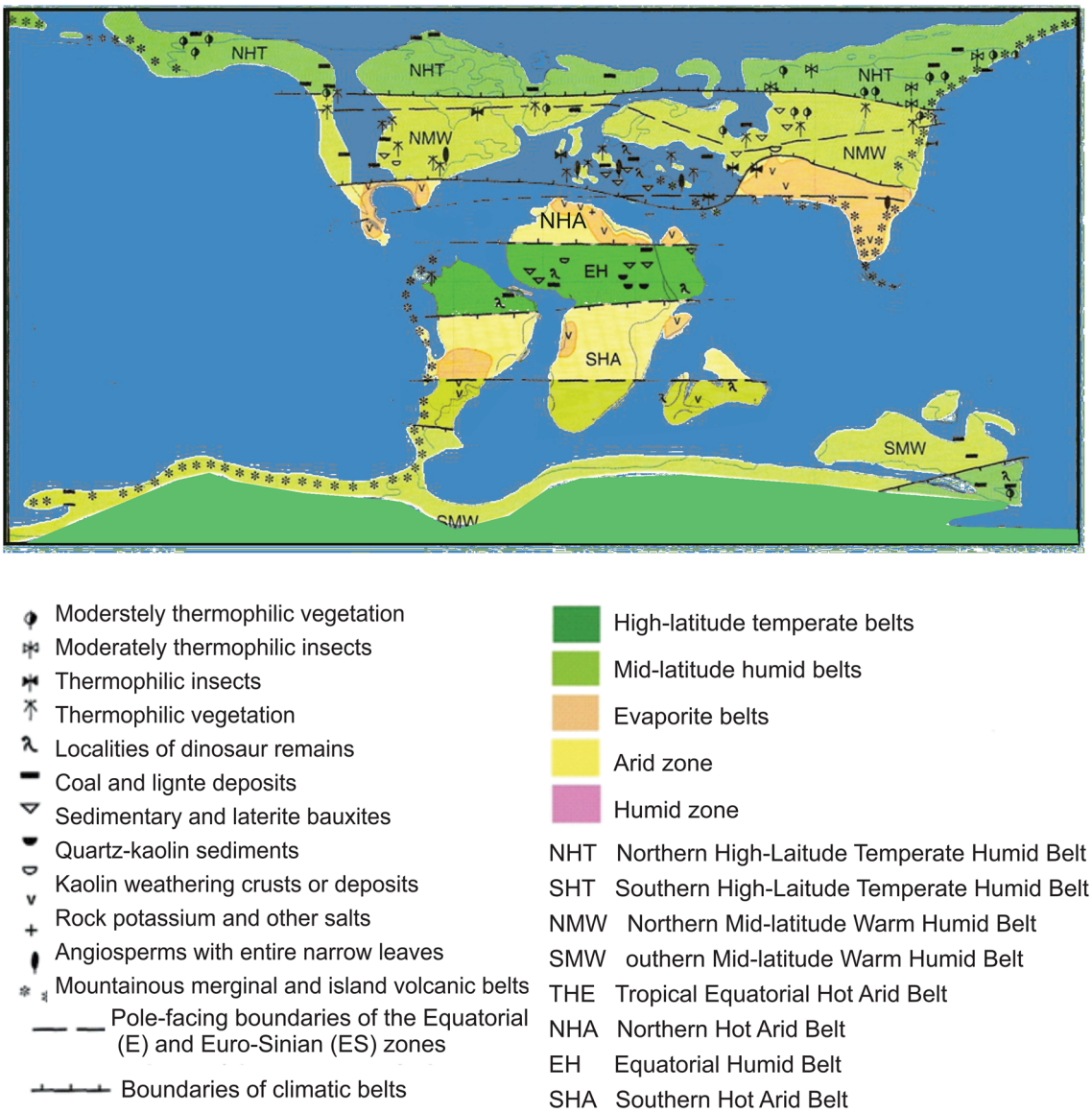

Fig. 15 Map of fossil and sedimentary climatic indicators prepared by Nikolai M. Chumakov. Adapted from Hay and Floegel (2012)

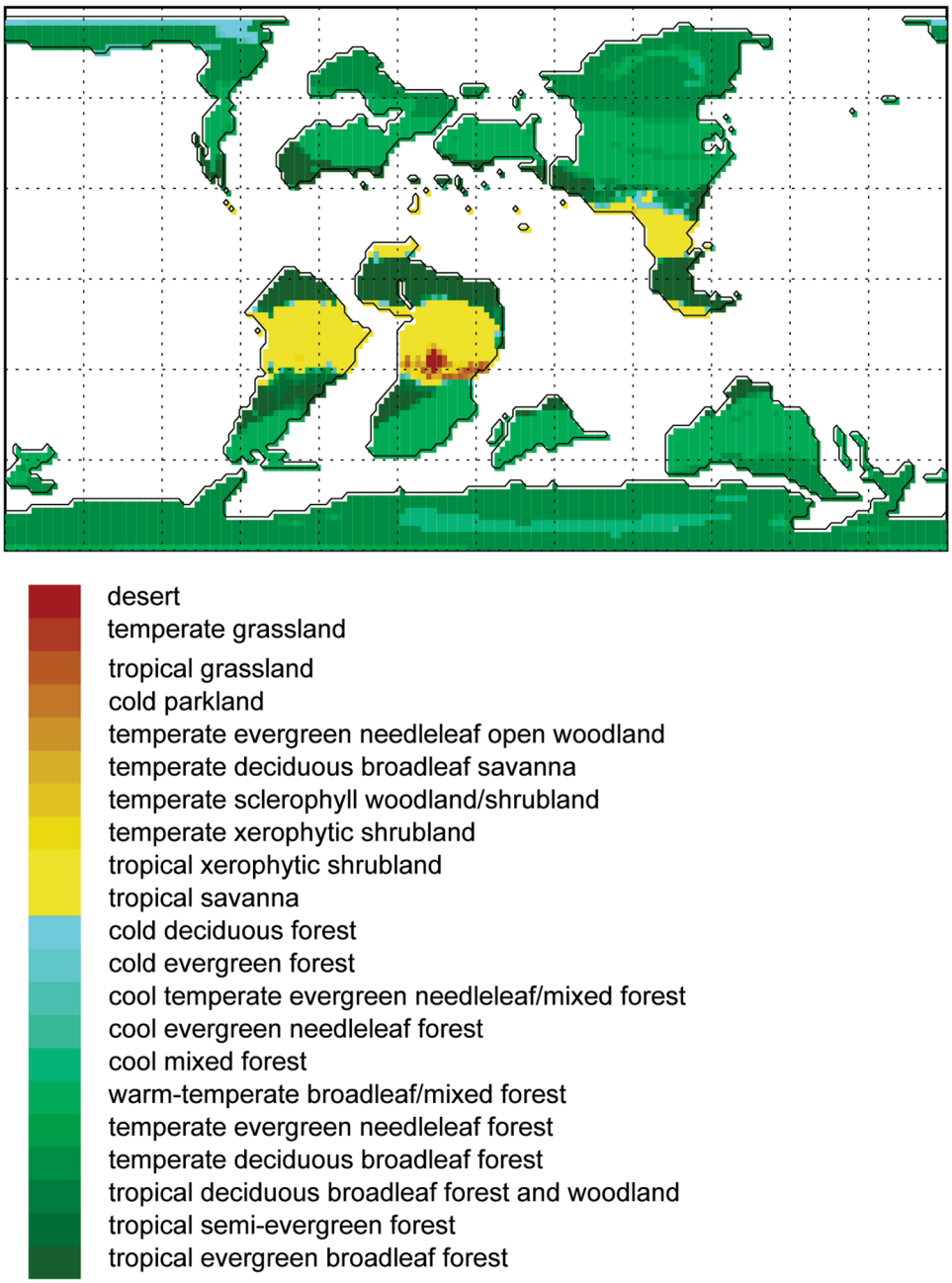

Fig. 16 Simulated distribution of land-surface biomes, simulated by the GCM and Biome4, for $8 \times CO_2$ 'equivalent' atmospheric greenhouse gas concentration and 75% wetland surfaces

widespread below freezing temperatures. The 8 × 'preindustrial CO_2 equivalent' simulation with 75% lakes, river surfaces, and wetlands produces an Arctic essentially free of below-freezing temperatures during northern hemisphere winter. With slightly higher CO_2 equivalent greenhouse gas concentrations, the wet areas on the continents could be reduced, but probably not much below 50%.

The simulations with 16 × 'preindustrial CO_2 equivalent' greenhouse gas concentrations are unrealistic. They all result in large areas in both hemispheres too warm to support plant

Fig. 17 Aerial view of the lower reaches of the Rio Tigre in Peru, a tributary of the Amazon, and its surrounding rainforest wetland. Image posted at several sites on the Internet. The Rio Tigre is muddy, carrying sediment eroded from the Andes, a 100 km to the west. The airline distance from the Rio Tigre to the mouth of the Amazon is about 2500 km. Following the meandering of the rivers, the distance is about 7500 km, all of it in rainforest wetlands

Fig. 18 Freshwater swamp forest in the Ganges–Brahmaputra delta of Bangladesh. Picture courtesy Wikipedia

Fig. 19 Swamp with trees. Figure courtesy Sciencing.com. Although the Cretaceous trees were different, this gives a good ground-level impression of what much of the humid belts of the Mid-Cretaceous might have been like

growth no matter how extensive the water surfaces might have been.

Effect of lakes, river surfaces, and wetlands on diurnal temperatures

Earth's warm climate states are often referred to as 'equable' (Barron 1983; Sloan and Barron 1990), referring to the decrease in meridional temperature gradient. However, the term can also be used with reference to the day–night temperature difference. Increasing water vapor content of the air not only reduces the meridional temperature gradient but reduces the range of diurnal temperatures, as shown in Fig. 13. The effect is small with an increase in wetlands to 25% but becomes much larger with increases to 50% and 75%.

Modern diurnal temperature differences are significantly larger than those for 8 × preindustrial CO_2 equivalent greenhouse gas concentrations with 50% and 75% wet surface areas on land (Fig. 14).

Comparison of model and geologic data

The most complete global account of fossil and sedimentary evidence for the Cenomanian 100.5–93.9 Ma was initially compiled by Chumakov (1995) and Chumakov et al. (1995) and subsequently reanalyzed by Chumakov (2004). A reproduction of the global map showing the distribution of these data was included in Hay and Floegel (2012) and is shown below (Fig. 15).

The climate simulations discussed above used a modification of the BIOME4 vegetation model (Kaplan et al. 2003), interactively coupled to the GCM. The biome vegetation model for 8 × CO_2 and 75% water-covered, low lying land is shown in Fig. 16. The biome classifications simulated by the model are determined by the fractional mix of plant functional types in each model grid cell. Although the terminologies are different, there is close correspondence with the distribution of geological data shown in Fig. 15.

Although the terminologies used are different, there is a close correspondence between the Chumakov data compilation and his interpretation of climatic zones and the biome vegetation model. Where was the water? The biome 'tropical evergreen broadleaf forest' corresponds closely to what is today called the 'várzea forest' or 'tropical rainforest' which is widespread in the Amazon Basin and other watersheds in the equatorial–subequatorial humid belt. Figures 17, 18 and 19 show what the rivers, rainforests and swamplands in this region look like today. In the Mid-Cretaceous the vegetation was different, but the overall situation was probably very much like what we see today.

As shown in Fig. 6, the area of lowland regions during the Mid-Cretaceous was about twice as large as that today. With

more intense and frequent rainfall, water surfaces would have been much larger.

Conclusions

The nature of the warm climates of the Cretaceous has been an enigma for over 40 years. Numerical models of the paleoclimate have consistently failed to agree with information from fossils and climate sensitive sediments.

One important problem, the 'cold continental interior paradox' (DeConto et al. 1999) has been solved by reconsideration of the age of areas uplifted by subduction along the northeastern Siberian continental margin.

Another problem, the apparent evidence for significant masses of ice on land during very warm periods has been solved by considering the effects of groundwater storage and release.

The problem of a warm Arctic, not previously solved by numerical simulations using increases in CO_2 equivalent greenhouse gas concentrations alone, has been solved by assuming that there were much more extensive wetlands (lakes, meandering rivers, swamps, and bogs) on the continents than has been previously assumed.

Using ~ 8 × preindustrial CO_2 equivalent greenhouse gas concentrations and assuming 50–75% wetlands on the continents reduces the meridional temperature gradients from the equatorial to polar regions and produces conditions compatible with fossil and sedimentological evidence.

The more extensive water surfaces were in rainforest-swamp biomes in the Equatorial and mid-latitude humid belts.

Acknowledgements We thank all of those who have helped in the development of the ideas presented herein. Donald S. Marszalek and Jim Stunkle read drafts and suggested improvements. Robert DeConto's work on Cretaceous climates originally supported by Grants from the US National Science Foundation. Sascha Flögel's work was supported by the German Science Foundation (SFB 754 sub-project A7). Ying Song's work has been supported by the China University of Petroleum (East China) in Qingdao. Andrei Stepashko is supported by the Kosygin Institute of Tectonics and Geophysics, Far East Division, Russian Academy of Sciences.

References

Alder JR, Hostetler SW, Pollard D, Schmittner A (2011) Evaluation of a present-day climate simulation with a new coupled atmosphere–ocean model GENMOM. Geosci Model Dev 4:69–83

Alley NF, Frakes LA (2003) First known Cretaceous glaciation: Livingston Tillite Member of the Cadna-owie Formation, South Australia. Aust J Earth Sci 50:139–144

Armor AB, Vereshchagin VN, Vinogradov AP (eds) (1966) Атлас литолого-палеографических карт СССР. Том 3. Триасовый, юрский и меловой периоды (Atlas of the Lithological–Paleogeographical Maps of the USSR. vol III: Triassic, Jurassic and Cretaceous Periods), p 80

Arthur MA, Dean WE, Schlanger SO (1985) Variations in the global carbon cycle during the Cretaceous related to climate, volcanism, and changes in atmospheric CO_2. In: Sundquist ET, Broecker WS (eds) The carbon cycle and atmospheric CO_2: natural variations archean to present, pp 504–529

Balukhovsky A, Floegel S, Hay WW, Madison A, Wold CN (2004) A paleogeographic map for the Lower Turonian. https://earthref.org/ERDA/220/

Barclay RS, Wing SL (2016) Improving the *Ginkgo* CO_2 barometer: implications for the early Cenozoic atmosphere. Earth Planet Sci Lett 439:158–171

Barron EJ (1983) Warm, equable Cretaceous, the nature of the problem. Earth Sci Rev 19:305–338

Barron EJ, Washington WM (1982) Atmospheric circulation during warm geologic periods: is the equator-to-pole surface-temperature gradient the controlling factor? Geology 10:633–636

Barron EJ, Washington WM (1984) The role of geographic variables in explaining paleoclimates; results from cretaceous climate model sensitivity studies. J Geophys Res 89:1267–1279

Barron EJ, Washington WM (1985) Warm Cretaceous climates: high atmospheric CO_2 as a plausible mechanism. In: Sundquist ET, Broecker WS (eds). The carbon cycle and atmospheric CO_2: natural variations archean to present, pp 546–553

Barron EJ, Thompson SL, Schneider SH (1981a) An ice-free Cretaceous? Results from climate model simulations. Science 212:501–508

Barron EJ, Harrison CGA, Sloan JL II, Hay WW (1981b) Paleogeography, 180 million years ago to the present. Ecl Geol Helvetiae 74:443–470

Barron EJ, Peterson WH, Pollard D, Thompson S (1993a) Past climate and the role of ocean heat transport: model simulations for the Cretaceous. Paleoceanography 8:785–798

Barron EJ, Fawcett PJ, Pollard D, Thompson S (1993b) Model simulations of Cretaceous climates: the role of geography and carbon dioxide [and Discussion]. Philos Trans R Soc Lond B Biol Sci 341:307–316

Barron EJ, Fawcett PJ, Peterson WH, Pollard D, Thompson SL (1995) A 'simulation' of Mid-Cretaceous climate. Paleoceanography 10:953–962

Bely VF (1997) The North Pacific refugium, and the problems of paleofloristics of the Middle Cretaceous in northeastern Asia. Pac Ocean Geol 16/6:102–113 **(in Russian: (Белый, В.Ф. (1997) Северо-Тихоокеанский рефугиум и проблемы палеофлоры среднего мела в северо-восточной Азии. Тихокеанская Геология 16/6: 102–113)**

Berner RA, Kothavala Z (2001) GEOCARB III: a revised model of atmospheric CO_2 over Phanerozoic time. Am J Sci 301:182–204

Bice KL, Norris RD (2002) Possible atmospheric CO_2 extremes of the Middle Cretaceous (late Albian–Turonian). Paleoceanography. https://doi.org/10.1029/2002PA000778

Bice KL, Huber BT, Norris RD (2003) Extreme polar warmth during the Cretaceous greenhouse? Paradox of the late Turonian $\delta^{18}O$ record at Deep Sea Drilling Project Site 511. Paleoceanography 18(1301):9:1–7. https://doi.org/10.1029/2002PA000848

Bice K, Birgel D, Meyers PA, Dahl KA, Hinrichs K-U, Norris RD (2006) A multiple proxy and model study of Cretaceous upper ocean temperatures and atmospheric CO_2 concentrations. Paleoceanography 21:17. https://doi.org/10.1029/2005PA001203. PA2002

Boyd ES, Peters JW (2013) New insights into the evolutionary history of biological nitrogen fixation. Front Microbiol 4:201. https://doi.org/10.3389/fmicb.2013.00201

Budyko MI, Ronov AB (1979) Evolution of the atmosphere in the Phanerozoic. Geochemistry 5:643–653 **(in Russian: Будыко МИ., Ронов АБ (1979) Эволюция атмосферы в фанерозое. Геохимия. №5: 643–653)**

Budyko MI, Ronov AB (1987) History of the earth's atmosphere. Springer, Heidelberg, 139 pp

Budyko MI, Ronov AB, Yanshin AL (1985) History of the atmosphere. Gidrometeoizdat 1985:207 **(in Russian: Будико, МИ Ронов, АБ Яншин АЛ (1985) История атмосферы. Гидрометеоиздать, 207 С.)**

Callander RA (1969) Instability and river channels. J Fluid Mech 36:465–480

Callander RA (1978) River meandering. Annu Rev Fluid Mech 10:129–158

Cantrill DJ, Hunter MA (2005) Macrofossil floras of the Latady Basin, Antarctic Peninsula. NZ J Geol Geophys 48:537–553

Chen L-Q, Li C-S, Chaloner WG, Beerling DJ, Sun Q-G, Collinson ME, Mitchell PL (2001) Assessing the potential for the stomatal characters of extant and fossil *Ginkgo* leaves to signal atmospheric CO_2 change. Am J Bot 88:1309–1315

Chumakov NM (1995) The problem of the warm biosphere. Stratigr Geol Correl 3:205–215

Chumakov NM (2004) Climatic zones and climate of the Cretaceous period. In: Semikhatov MA, Chumakov NM (eds) Climate in the epochs of major biospheric transformations. Transactions of the Geological Institute of the Russian Academy of Sciences, vol 550. Nauka, Moscow, pp 105–123 **(in Russian)**

Chumakov NM, Zharkov MA, Herman AB, Doludenko MP, Kalandadze NN, Lebedev EA, Ponomarenko AG, Rautian AS (1995) Climate belts of the Mid-Cretaceous time. Stratigr Geol Correl 3:241–260

Cloetingh S, Haq BU (2015) Inherited landscapes and sea level change. Science 347:1258375

Conrad CP (2013) The solid Earth's influence on sea level. GSA Bull 125:1027–1052. https://doi.org/10.1130/B30764.1

Constantine JA, Dunne TS, Piégay H, Kondolf GM (2010) Controls on the alluviation of oxbow lakes by bed-material load along the Sacramento River, California. Sedimentology 57:389–407

Crafts-Brandner SJ, Salvucci ME (2000) Rubisco activase constrains the photosynthetic potential of leaves at high temperature and CO_2. Proc Natl Acad Sci 97:13430–13435

Davies NS, Gibling MR, Rygel MC (2011) Alluvial facies evolution during the Palaeozoic greening of the continents: case studies, conceptual models and modern analogues. Sedimentology 58:220–258

DeConto RM (1996) Late Cretaceous climate, vegetation and ocean interactions, an Earth system approach to modeling an extreme climate [Ph.D. Thesis]: Boulder, University of Colorado, p 236

DeConto RM, Hay WW, Bergengren JC (1998) Modeling Late Cretaceous climate and vegetation. Zent Geol Paläontol 1996(11/12):1433–1444

DeConto RM, Hay WW, Thompson SL, Bergengren J (1999) Late Cretaceous climate and vegetation interactions: the cold continental interior paradox. In: Barrera E, Johnson C (eds) Evolution of the Cretaceous Ocean/climate system, vol 332. Geological Society of America Special Paper, Boulder, pp 391–406

DeConto RM, Brady E, Bergengren J, Hay WW (2000a) Late Cretaceous climate, vegetation, and ocean interactions. In: Huber BT, MacLeod KG, Wing SL (eds) Warm Climates in Earth History. Cambridge University Press, Cambridge, pp 275–297

DeConto RM, Thompson SL, Pollard D (2000b) Recent advances in paleoclimate modeling: toward better simulations of warm paleoclimates. In: Huber BT, MacLeod KG, Wing SL (eds) Warm Climates in Earth History. Cambridge University Press, Cambridge, pp 21–49

DeConto RM, Galeotti S, Pagani M, Tracy D, Schaefer K, Zhang T, Pollard D, Bee DJ (2012a) Past extreme warming events linked to massive carbon release from thawing permafrost. Nature 484:87–91

DeConto RM, Galeotti S, Pagani M, Tracy D, Schaefer K, Zhang T, Pollard D, Bee DJ (2012b) Corrigendum: Past extreme warming events linked to massive carbon release from thawing permafrost. Nature 490:292

DeLurio JL, Frakes LA (1999) Glendonites as a paleoenvironmental tool: implications for early Cretaceous high latitude climates in Australia. Geochim Cosmochim Acta 63:1039–1048

DeMeo J (1989) Desert expansion and drought: environmental crisis, Part I. J Orgonom 23:15–26

Dewey JF, Burke K (1974) Hot spots and continental breakup: implications for collisional orogeny. Geology 2:57–60

Donnadieu Y, Pierrehumbert R, Jacob R, Fluteau F (2006) Modelling the primary control of paleogeography on Cretaceous climate. Earth Planet Sci Lett 248:426–437

Donnelly TW (1982) Worldwide continental denudation and climatic deterioration during the late Tertiary: evidence from deep-sea sediments. Geology 10:451–454

Downing JA, Prairie YT, Cole JJ, Duarte CM, Tranvik LJ, Striegl RG, McDowell WH, Kortelainen P, Caraco NF, Melack JM, Middelburg JJ (2006) The global abundance and size distribution of lakes, ponds, and impoundments. Limnol Oceanogr 51:2388–2397

Downing JA, Cole JJ, Duarte CM, Middelburg JJ, Melack JM, Prairie YT, Kortelainen P, Striegl RG, McDowell WH, Tranvik LJ (2012) Global abundance and size distribution of streams and rivers. Inland Waters 2:229–236

Ellis RJ (2010) Tackling unintelligent design. Nature 463:164–165

Fisk HN (1944) Geological Investigation of the Alluvial Valley of the Lower Mississippi Valley. Mississippi River Commission Publication 1. US Army Corps of Engineers, Vicksburg, p 78 + 33 plates

Floegel S, Hay WW, DeConto RM, Balukhovsky AN (2005) Formation of sedimentary bedding couplets in the Western Interior Seaway of North America—implications from climate system modeling. Palaeogeogr Palaeoclimatol Palaeoecol 218:125–143

Flögel S (2001) On the influence of precessional Milankovitch cycles on the Late Cretaceous climate system: comparison of GCM-results, geochemical, and sedimentary proxies for the Western Interior Seaway of North America. Doctoral Thesis, Faculty of Mathematics and Natural Sciences of the Christian-Albrecht's-University, Kiel, Germany, p 236

Flögel S, Parkin G, Pollard D, Dullo W-Chr, Wagner T (2010) Simulating zonal scale shifts in the partitioning of surface and subsurface freshwater flow in response to increasing pCO_2. Clim Dyn 37:1565–1573. https://doi.org/10.1007/s00382-010-0929-5

Flögel S, Wallmann K, Poulsen CJ, Zhou J, Oschlies A, Voigt S, Kuhnt W (2011a) Simulating the biogeochemical effects of volcanic CO_2 degassing on the oxygen-state of the deep ocean during the Cenomanian/Turonian Anoxic Event (OAE2). Earth Planet Sci Lett 305:371–384. https://doi.org/10.1016/j.epsl.2011.03.018

Flögel S, Wallmann K, Kuhnt W (2011b) Cool episodes in the Cretaceous—exploring the effects of physical forcings on Antarctic snow accumulation. Earth Planet Sci Lett 307:279–288

Frakes LA, Francis JE (1988) A guide to Phanerozoic cold polar climates from high-latitude ice-rafting in the Cretaceous. Nature 333:547–549

Francis JE, Poole I (2002) Cretaceous and early Tertiary climates of Antarctica: evidence from fossil wood. Palaeogeogr Palaeoclimatol Palaeoecol 182:47–64

Francis JE, Pirrie D, Crame JA (eds) (2006) Cretaceous-tertiary high-latitude palaeoenvironments, James Ross Basin, Antarctica, vol 258. Geological Society, London, Special Publications, London, p 200. ISBN-10: 1862391971, ISBN-13: 978-1862391970

Fredsøe J (1978) Meandering and braiding of rivers. J Fluid Mech 84:609424

Grasby SF, McCune GE, Beauchamp B, Galloway JM (2017) Lower Cretaceous cold snaps led to widespread glendonite occurrences in the Sverdrup Basin, Canadian High Arctic. Geol Soc Am Bull B31600-1:17. https://doi.org/10.1130/B31600.1

Greiner B, Neugebauer J (2013) The rotations opening the Central and Northern Atlantic Ocean: compilation, drift lines, and flow lines. Int J Earth Sci 102:1357–1376

Greinert J, Derkachev A (2004) Glendonites and methane-derived Mg-calcites in the Sea of Okhotsk, Eastern Siberia: implications of a venting-related ikaite/glendonite formation. Mar Geol 204:129–144

Hansen KW, Wallman K (2003) Cretaceous and Cenozoic evolution of seawater composition, atmospheric O_2 and CO_2: a model perspective. Am J Sci 303:94–148

Haq BU (2014) Cretaceous eustasy revisited. Glob Planet Change 113:44–58

Harrison CGA, Miskell KJ, Brass GW, Saltzman ES, Sloan IIJA (1983) Continental hypsography. Tectonics 2:357–377

Hasegawa H, Tada R, Jiang X, Suganuma Y, Imsamut S, Charusiri P, Ichinnorov N, Khand Y (2012) Drastic shrinking of the Hadley circulation during the mid-Cretaceous Supergreenhouse. Clim Past 8:1323–1337

Hay WW (1981) Sedimentological and geochemical trends resulting from the breakup of Pangaea. Oceanol Acta 4/Suppl:135–147

Hay WW (1994) Pleistocene-Holocene fluxes are not the earth's norm. In: Hay WW, Usselmann T (eds) Material fluxes on the surface of the earth. Studies in geophysics. National Academy Press, Washington D.C., pp 15–27

Hay WW (1998) Detrital sediment fluxes from continents to oceans. Chem Geol 145:287–323

Hay WW (2008) Evolving ideas about the Cretaceous climate and ocean. Cretac Res 29:725–753

Hay WW (2009) Cretaceous oceans and ocean modelling. In: Hu X, Wang C, Scott RW, Wagreich M, Jansa L (eds) Cretaceous oceanic red beds: stratigraphy, composition, origins and paleoceanographic and paleoclimatic significance, vol 91. SEPM (Society for Sedimentary Geology) Special Publication, Tulsa, pp 243–271 **(ISBN 978-1-56576-135-3)**

Hay WW (2016) Experimenting on a small planet. A history of scientific discoveries, a future of climate change and global warming. Springer, Berlin, p 819

Hay WW (2017) Toward understanding Cretaceous climate—an updated review. Sci China Earth Sci 60:5–19

Hay WW, Floegel S (2012) New thoughts about the Cretaceous climate and oceans. Earth Sci Rev 115:262–272

Hay WW, Leslie MA (1990) Could possible changes in global groundwater reservoir cause eustatic sea-level fluctuations? In: Revelle R (ed) (Panel Chairman), Sea—level change. National Academy Press, Washington D.C., pp 161–170

Hay WW, Southam JR (1977) Modulation of marine sedimentation by the continental shelves. In: Anderson NR, Malahoff A (eds) The fate of fossil fuel CO_2 in the oceans. Marine science series 6. Plenum Press, New York, pp 569–604

Hay WW, Usselmann T (eds) (1994) Material fluxes on the surface of the earth. Studies in geophysics. National Academy Press, Washington D.C., p 185

Hay WW, Barron EJ, Behensky JF Jr, Sloan JLII (1982) Triassic–Liassic paleoclimatology and sedimentation in proto-Atlantic rifts. Palaeogeogr Palaeoclimatol Palaeoecol 40:13–30

Hay WW, Shaw CA, Wold CN (1989) Mass-balanced paleogeographic maps: background and input requirements. In: Cross T (ed) Quantitative dynamic stratigraphy. Plenum Press, New York, pp 261–275

Hay WW, Eicher DL, Diner R (1993) Physical oceanography and water masses of the Cretaceous Western Interior Seaway. In: Caldwell WEG, Kauffman EG (eds) Evolution of the Western Interior Basin, vol 39. Geological Association of Canada, Special Paper, Canada, pp 297–318

Herman AB (1994) A review of late Cretaceous Floras and climates of Arctic Russia. In: Boulter MC, Fischer HC (eds) Cenozoic plants and climates of the Arctic. Springer, Berlin, pp 127–149

Herman AB (1999a) Cretaceous flora of the Anadyr–Koryak subregion (North-Eastern Russia) systematic composition, age, stratigraphic and florogenic significance [Герман А.Б., (1999) Меловая флора Анадырско-Корякского субрегиона (Северо-Восток России): систематический состав возраст, стратиграфическое и флорогенетическое значение]. Trans Russ Acad Sci Geol Inst 529:122 **(in Russian)**

Herman AB (1999b) Composition and age of the Grebenka Flora from the Anadyr River area (the Middle Cretaceous, North-eastern Russia). Stratigr Geol Correlat 7:265–278 **(in Russian: Герман А.Б, (1999) Состав и возраст флоры Гребенки из района реки Анадырь (средний мел, северо-восток России. Стратиграфия. Геологическая корреляция 7: 265–278 С)**

Herman AB, Spicer RA (1996) Palaeobotanical evidence for a warm Cretaceous Arctic Ocean. Nature 380:330–333

Herman AB, Spicer RA (1997) New quantitative palaeoclimate data for the Late Cretaceous Arctic: evidence for a warm polar ocean. Palaeogeogr Palaeoclimatol Palaeoecol 128:227–251

Herman AB, Spicer RA (2010) Mid-Cretaceous floras and climate of the Russian high Arctic (Novosibirsk Islands, Northern Yakutiya). Palaeogeogr Palaeoclimatol Palaeoecol 295:409–422

Hill RD, Rinker RG, Wilson HD (1980) Atmospheric nitrogen fixation by lightning. J Atmos Sci 37:179–192

Houghton JT, Jenkyns GJ, Ephraums JJ (1990) Climate change—the IPCC assessment. Cambridge University Press, Cambridge, 365 pp

Huang Y, Shahabadi MB (2014) Why logarithmic? A note on the dependence of radiative forcing on gas concentration. J Geophys Res Atmos 119:13,683–13,689. https://doi.org/10.1002/2014JD022466

Iglesias A, Zamuner AB, Poiré G, Larriestra F (2007) Diversity, taphonomy and palaeoecology of an angiosperm flora from the Cretaceous (Cenomanian–Coniacian) in southern Patagonia. Argent Palaeontol 50:445–466

Jackson JR (1834) Hints on the subject of geographical arrangement and nomenclature. J R Geogr Soc Lond 4:72–88

Jacobs DK, Sahagian DL (1993) Climate induced fluctuations in sea level during non-glacial times. Nature 361:710–712

Jacobs DK, Sahagian DL (1995) Milankovitch fluctuations in sea level and recent trends in sea-level change: ice may not always be the answer. In: Haq BU (ed) Sequence stratigraphy and depositional response to eustatic, tectonic and climatic forcing. Kluwer Academic Publishers, Dordrecht, pp 329–366

Jensen RG (2000) Activation of Rubisco regulates photosynthesis at high temperature and CO_2. Proc Natl Acad Sci 97:12937–12938

Kaplan JO (2001) Geophysical applications of vegetation modeling. Ph.D. Thesis, Lund University, Lund, Sweden, p 129

Kaplan JO, Bigelow NH, Prentice IC, Harrison SP, Bartlein PJ, Christensen TR, Cramer W, Matveyeva NV, McGuire AD, Murray DF, Razzhivin VY, Smith B, Walker DA, Anderson PM, Andreev AA, Brubaker LB, Edwards ME, Lozhkin AV (2003) Climate change and Arctic ecosystems: 2. modeling, paleodata-model comparisons, and future projections. J Geophys Res 108(D19):8171. https://doi.org/10.1029/2002JD002559

Kazmin VG, Napatov LM (eds) (1998) Палеогеографическая Атлас Северного Евразия—Paleogeographic Atlas of Northern Eurasia: Institute of Tectonics of the Lithospheric Plates. Russian Academy of Natural Sciences, Moscow **(20 maps + legend)**

Kemper E (1987) Das Klima der Kreide-Zeit. Geol Jahrbuch Reihe A 96:185 pp

Kemper E, Schmitz HH (1981) Glendonite ~ Indikatoren des polarmarinen Ablagerungsmilieus. Geol Rundsch 70:759–778

Kidder DL, Worsley TR (2010) Phanerozoic Large Igneous Provinces (LIPs), HEATT (Haline Euxinic Acidic Thermal Transgression) episodes, and mass extinctions. Palaeogeogr Palaeoclimatol Palaeoecol 295:162–191

Kidder DL, Worsley TR (2012) A human-induced hothouse climate? GSA Today 22/2:11. https://doi.org/10.1130/G131A.1

Kiehl JT, Hack JJ, Bonan GB, Boville BA, Williamson DL, Raschet PJ (1998) The National Center for Atmospheric Research Community Climate Model: CCM3*. J Clim 11:1131–1149

Kinsman DJJ (1975) Rift valley basins and sedimentary history of trailing continental margins. In Fischer AG, Judson S (eds) Petroleum and global tectonics. Princeton University Press, Princeton, pp 83–126

Koch BE (1964) Review of fossil floras and nonmarine deposits of West Greenland. Geol Soc Am Bull 75:535–548

Krause DW, Rogers RR, Forster CA, Hartman JH, Buckley GA, Sampson SD (1999) The Late Cretaceous Vertebrate Fauna of Madagascar: implications for Gondwanan Paleobiogeography. GSA Today 9(8):1–7

Krause DW, O'Connor PM, Rogers KC, Sampson SD, Buckley GA, Rogers RR (2006) Late Cretaceous terrestrial vertebrates from Madagascar: implications for Latin American biogeography. Ann Missouri Bot Garden 93:178–208

Kump LR, Pollard D (2008) Amplification of Cretaceous warmth by biological cloud feedbacks. Science 320:195

Latrubesse EM (2008) Patterns of anabranching channels: the ultimate end-member adjustment of mega rivers. Geomorphology 101:130–145

Leeder M (2007) Cybertectonic Earth and Gaia's weak hand: sedimentary geology, sediment cycling and the Earth system. J Geol Soc 164:277–296

Legates DR, Willmott CJ (1990) Mean seasonal and spatial variability in gauge-corrected, global precipitation. Int J Climatol 10:111–127

Leopold L (1953) Downstream change in velocity of rivers. Am J Sci 251:606–624

Leopold LB, Wolman MG (1957) River channel patterns—braided, meandering, and straight. US Geol Surv Profess Pap 282B:39–85

Leopold L, Wolman MG (1960) River meanders. Geol Soc Am Bull 71:769–794

Li W, Li L, Fu R, Deng Y, Wang H (2011) Changes to the North Atlantic subtropical high and its role in the intensification of summer rainfall variability in the Southeastern United States. J Clim 24:1499–1506

Li W, Li L, Ting M, Liu Y (2012) Intensification of Northern Hemisphere subtropical highs in a warming climate. Nat Geosci 5:830–834

Liu L, Spasojević S, Gurnis M (2008) Reconstructing Farallon Plate subduction beneath North America back to the Late Cretaceous. Science 322:934–938

Liu C, Young AL, Starling-Windhof A, Bracher A, Saschenbrecker S, Rao BV, Rao KV, Berninghausen O, Mielke T, Hartl FU, Beckmann R, Hayer-Hartl M (2010) Coupled chaperone action in folding and assembly of hexadecameric Rubisco. Nature 463:197–202

Liu S, Nummedal D, Liu L (2011) Migration of dynamic subsidence across the Late Cretaceous United States Western Interior Basin in response to Farallon plate subduction. Geology 39:555–558

Makaske B (2001) Anastomosing rivers: a review of their classification, origin and sedimentary products. Earth Sci Rev 53:149–196

Manfroi J, Dutra TL, Gnædinger S, Uhl D, Jasper A (2015) The first report of a Campanian palaeo-wildfire in the West Antarctic Peninsula. Palaeogeogr Palaeoclimatol Palaeoecol 418:12–18

Markwick PJ, Valdes PJ (2004) Palaeo-digital elevation models for use as boundary conditions in coupled ocean–atmosphere GCM experiments: a Maastrichtian (Late Cretaceous) example. Palaeogeogr Palaeoclimatol Palaeoecol 213:37–63

Markwick PJ, Rowley DB, Ziegler AM, Hulver P, Valdes PJ, Sellwood BJ (2000) Late Cretaceous and Cenozoic global palaeogeographies: mapping the transition from a "hot-house" to an "ice-house" world. GFF 122:103

Melton JR, Wania R, Hodson EL, Poulter B, Ringval B, Spahni R, Bohn T, Avis CA, beerling DJ, Chan G, Eliseev AV, Denisov SN, Hopcroft DO, Lettemmaier DP, Riley WJ, Singarayer JS, Subin ZM, Tian H, Zürcher, Brovkin V, van Bodegom PM, Kleinen T, Yu ZC, Kaplan JO (2013) Present state of global wetland extent and wetland methane modelling: conclusions from a model intercomparison project (WETCHIMP). Biogeosciences 10:753–788. https://doi.org/10.5194/bg-10-753-2013

Miller KG (2009) Broken greenhouse windows. Nat Geosci 2:465–466

Miller KG, Sugarman PJ, Browning JV, Kominz MA, Hernández JC, Olsson RK, Wright JD, Feigenson MD, Van Sickel W (2003) Late Cretaceous chronology of large, rapid sea-level changes: glacioeustasy during the greenhouse world. Geology 31:585–588

Miller KG, Kominz MA, Browning JV, Wright JD, Mountain GS, Katz ME, Sugarman PJ, Cramer BS, Christie-Blick N, Pekar SF (2005) The phanerozoic record of global sea-level change. Science 310:1293–1298

Müller RD, Sdrolias M, Gaina C, Steinberger B, Heine C (2008) Long-term sea-level fluctuations driven by ocean basin dynamics. Science 319:1357–1362

Mutterlose J, Bornemann A, Herrle J (2008) The Aptian–Albian cold snap: evidence for "mid" Cretaceous icehouse interludes. Neues Jahrbuch Geol Paläontol Abhandlungen 252:217–225

Neugebauer J, Greiner B (2014) Reply to: Frisch and Dawes (DOI 10.1007/s00531-013-0980–7) discussion on the rotations opening the Central and Northern Atlantic Ocean: compilation, drift lines, and flow lines (DOI 10.1007/s00531-012-0860-6). Int J Earth Sci 103:971–976

Niezgodzki I, Knorr G, Lohmann G, Tyszka J, Markwick PJ (2017) Late Cretaceous climate simulations with different CO_2 levels and subarctic gateway configurations: a model-data comparison. Paleoceanography 32:19. https://doi.org/10.1002/2016PA003055

Nordenskiöld AE (1870) Redogörelse för en expedition till Grönland ar 1870. Kongliga Svenska Aakademie Ofversikt 10:923–1082

Nordenskiöld A (1872) I—Account of an expedition to Greenland in the year 1870. Geol Mag 9:289–306. https://doi.org/10.1017/S001675680046513

Norris RD, Bice KL, Magno EA, Wilson PA (2002) Jiggling the tropical thermostat in the Cretaceous hothouse. Geology 30:299–302

Otto-Bliesner BL, Upchurch GR Jr (1997) Vegetation-induced warming of high-latitude regions during the Late Cretaceous period. Nature 385:804–807

Parrish JT, Spicer RA (1988) Late Cretaceous terrestrial vegetation: a near-polar temperature curve. Geology 16:22–25

Pauly H (1963) "Ikaite" a new mineral from Greenland. Arctic 16:263–264

Poole I (2000) Fossil angiosperm wood; its role in reconstruction of biodiversity and palaeoenvironment. Int J Linnean Soc 134:361–381

Poole I, Cantrill DJ (2006) Cretaceous and Cenozoic vegetation of Antarctica integrating the fossil wood record. Geol Soc Lond Spec Publ 258:63–81

Poole I, Francis JE (2000) The first record of fossil wood of Winteraceae from the Upper Cretaceous of Antarctica. Ann Bot 85:307–315

Poole I, Richter HG, Francis JE (2000) Evidence for Gondwanan origins for Sassafras (Lauraceae)? Late Cretaceous fossil wood of Antarctica. IAWA J 21:463–475

Price GD, Nunn EV (2010) Valanginian isotope variation in glendonites and belemnites from Arctic Svalbard: transient glacial temperatures during the Cretaceous greenhouse. Geology 38:251–254

Ramanathan V, Vogelmann AM (1997) Greenhouse effect, atmospheric solar absorption and the earth's radiation budget: from the Arrhenius–Langley Era to the 1990s. Ambio 26:38–46

Retallack GJ (2001) A 300-million-year record of atmospheric carbon dioxide from fossil plant cuticles. Nature 411:287–290

Rodellas VI, Garcia-Orellanaa J, Masquéa P, Feldmane M, Weinsteine Y (2015) Submarine groundwater discharge as a major source of nutrients to the Mediterranean Sea. Proc Natl Acad Sci 112:3926–3930

Rogers JJW, Santosh M (2013) Supercontinents in Earth history. Gondwana Res 6:357–368

Rogov MA, Zakharov VA (2010) Jurassic and lower Cretaceous glendonite occurrences and their implication for Arctic paleoclimate reconstructions and stratigraphy. Earth Sci Front 17:345–347

Ronov AB (1982) The Earth's sedimentary shell (quantitative patterns of its structure, composition, and evolution). Int Geol Rev 24:1313–1363, 1365–1388

Ronov AB (1993) Стратисфера—Или Осадочная Оболочка Земли (количественное исследование) [Stratisphere—or Sedimentary Shell of the Earth (quantitative research)]. Nauka, Moscow, p 144 **(ISBN 5-02-003117-8)**

Ronov AB (1994) Phanerozoic transgressions and regressions on the continents; a quantitative approach based on areas flooded by the sea and areas of marine and continental deposition. Am J Sci 294:777–801

Ronov AB, Khain VE, Seslavinsky KB (1984) Atlas of lithological–paleogeographical maps of the world: late Precambrian and Paleozoic of continents. Leningrad, Leningradskoe kartograficheskoe fabrike. VSEGEI 1984:70

Ronov AB, Khain VE, Balukhovsky AN (1989) In: Barsukhov VL, Laviorov NP (eds) Atlas of Lithological–paleogeographical maps of the world: mesozoic and cenozoic of continents and oceans. Editorial Publishing Group, Moscow, p 79

Rosgen DL (1994) A classification of natural rivers. Catena 22:169–199

Royer DL, Berner RA, Beerling DJ (2001) Phanerozoic atmospheric CO_2 change: evaluating geochemical and paleobiological approaches. Earth Sci Rev 54:349–392

Royer DL, Berner RA, Park J (2007) Climate sensitivity constrained by CO_2 concentrations over the past 420 million years. Nature 466:530–532

Royer DL, Pagani M, Beerling DJ (2012) Geobiological constraints on earth system sensitivity to CO_2 during the Cretaceous and Cenozoic. Geobiology 10:298–310

Sames B, Wagreich M, Wendler JE, Haq BU, Conrad CP, Melinte-Dobrinescu MC, Hu X, Wendler L, Wolfgring E, Yilmaz I, Zorina SO (2016) Review: short-term sea-level changes in a greenhouse world—a view from the Cretaceous. Palaeogeogr Palaeoclimatol Palaeoecol 441:393–411.j

Schaller M, von Blanckenburg F, Hovius N, Kubik PW (2001) Large-scale erosion rates from in situ-produced cosmogenic nuclides in European river sediments. Earth Planet Sci Lett 188:441–458

Schneider SH, Thompson SL, Barron EJ (1985) Mid-Cretaceous continental surface temperatures: are high CO_2 concentrations needed to simulate above-freezing winter conditions?. In: Sundquist ET, Broecker WS (eds). The carbon cycle and atmospheric CO_2: natural variations archean to present, pp 554–559

Schultz BP (2009) Pseudomorph after ikaite—called Glendonite is it a geological thermometer in cold sediments or geological oddity as it occurs close to PETM in the Fur formation. IOP Conf Ser Earth Environ Sci 6:P07.47. https://doi.org/10.1088/1755-1307/6/7/072059

Schumm SA (1985) Patterns of alluvial rivers. Annu Rev Earth Planet Sci 13:5–27

Selleck BW, Carr PF, Jones BG (2007) A review and synthesis of glendonites (pseudomorphs after ikaite) with new data: assessing applicability as recorders of ancient coldwater conditions. J Sedim Res 77:980–991

Sellers PJ, Bounoua GJ, Collatz DA, Randall DA, Los Dazlich SO, Berry JA, Fung I, Tucker CJ, Field CB, Jensen. TG (1996) Comparison of radiative and physiological effects of doubled atmospheric CO_2 on climate. Science 271:1402–1406

Sellwood BW, Valdes PJ (2006) Mesozoic climates: general circulation models and the rock record. Sed Geol 190:269–287

Sewall JO, van de Wal RSW, van der Zwan K, van Oosterhout C, Dijkstra HA, Scotese CR (2007) Climate model boundary conditions for four Cretaceous time slices. Clim Past 3:647–657

Shaw CA, Hay WW (1989) Mass-balanced paleogeographic maps: modeling program and results. In: Cross T (ed) Quantitative dynamic stratigraphy. Plenum Press, New York, pp 277–291

Sloan LC, Barron EJ (1990) Equable climates during earth history. Geology 18:489–492

Sloan LC, Pollard D (1998) Polar stratospheric clouds: a high latitude warming mechanism in an ancient greenhouse world. Geophys Res Lett 25:3517–3520

Smith A, Briden J (1977) Mesozoic cenozoic paleocontinental maps. Cambridge University Press, Cambridge, p 64

Song Y, Ren J, Stepashko AA, Li J (2014) Post-rift geodynamics of the Songliao Basin, NE China: origin and significance of T11 (Coniacian) unconformity. Tectonophysics 634:1–18

Song Y, Stepashko AA, Ren J (2015) The Cretaceous climax of compression in Eastern Asia: u age 87–89 Ma (late Turonian/Coniacian), Pacific cause, continental consequences. Cretac Res 55:262–284

Southam JR, Hay WW (1981) Global sedimentary mass balance and sea level changes. In: Emiliani C (ed) The sea, "The Oceanic Lithosphere": 1617–1684, 10 tables, 20 figs. Wiley, New York

Spicer RA, Herman AB (2010) The Late Cretaceous environment of the Arctic: a quantitative reassessment based on plant fossils. Paleogeogr Paleoclimatol Paleoecol 295:423–442

Spicer RA, Parrish JT (1987) Plant megafossils, vertebrate remains, and paleoclimate of the Kogosukruk Tongue (Late Cretaceous), North Slope, Alaska. US Geol Surv Circ 993(1987):47–48

Spicer RA, Ahlberg A, Herman AB, Kelley SP, Raikevich MI, Rees PM (2002) Palaeoenvironment and ecology of the middle Cretaceous Grebenka flora of northeastern Asia. Paleogeogr Paleoclimatol Paleoecol 184:65–105

Spicer RA, Ahlberg A, Herman AB, Hofmann C-C, Raikevich M, Valdes PJ, Markwick PJ (2008) The Late Cretaceous continental interior of Siberia: a challenge for climate models. Earth Planet Sci Lett 267:228–235

Stepashko AA (2009) Cretaceous seamounts: record of the extension history of the Pacific plate. In: Marturino L, Puopolo K (eds) New oceanography research developments: marine chemistry, ocean floor analyses and marine phytoplankton, pp 249–267

Stølum H-H (1998) Platform geometry and dynamics of meandering rivers. Geol Soc Am Bull 110:185–198

Suess E (2014) Marine cold seeps and their manifestations: geological control, biogeo-chemical criteria and environmental conditions. Int J Earth Sci 103:1889–1916. https://doi.org/10.1007/s00531-014-1010-0

Suess E, Balzer W, Hesse K-F, Müller PJ, Ungerer CA, Wefer G (1982) Calcium carbonate hexahydrate from organic-rich sediments

of the Antarctic shelf: precursors of glendonites. Science 216:1128–1131
Tarduno JSA, Brinkman DB, Renne PR, Cottrell RD, Scher H, Castillo P (1998) Evidence for extreme climatic warmth from Late Cretaceous Arctic Vertebrates. Science 282:2241–2244
Teichert BMA, Luppold FW (2013) Glendonites from an Early Jurassic methane seep—climate or methane indicators? Palaeogeogr Palaeoclimatol Palaeoecol 390:81–93
Termier H, Termier G (1952) Histoire géologique de la Biosphére. Masson & Cie, Paris, 721 pp
Termier H, Termier G (1960) Atlas de Paléogéographie. Masson & Cie, Paris, 99 pp
Thompson SL, Pollard D (1995a) A global climate model (GENESIS) with a land-surface transfer scheme (LSX). Part I: Present climates simulation. J Clim 8:732–761
Thompson SL, Pollard D (1995b) A global climate model (GENESIS) with a land-surface transfer scheme (LSX). Part 2: CO_2 sensitivity. J Clim 8:1104–1121
Thompson SL, Pollard D (1997) Greenland and Antarctic mass balances for present and doubled atmospheric CO_2 from the GENESIS version-2 global climate model. J Clim 10:871–900
Thorne BL, Grimaldi DA, Krishna K (2000) Early fossil history of the termites. In: Abe T, Bignell DE, Higashi M (eds) Termites: evolution, sociality, symbioses, ecology. Springer, Dordrecht, pp 77–94
Turner RE, Rabalais NN (2003) Linking landscape and water quality in the Mississippi River basin for 200 years. Bioscience 53:563–572
Upchurch GR Jr, Otto-Bliesner BL, Scotese CR (1998) Vegetation–atmosphere interactions and their role in global warming during the latest Cretaceous. Philos Trans R Soc Lond Ser B 353:97–112
Upchurch GR Jr, Otto-Bliesner BL, Scotese CR (1999) Terrestrial vegetation and its effects on climate during the latest Cretaceous.. In: Barrera E, Johnson C (eds) Evolution of the cretaceous ocean/climate system, vol 332. Geological Society of America Special Paper, Boulder, pp 407–426
Upchurch GR Jr, Kiehl J, Shields C, Scherer J, Scotese C (2015) Latitudinal temperature gradients and high-latitude temperatures during the latest Cretaceous: congruence of geologic data and climate models. Geology 43:683–686. https://doi.org/10.1130/G36802.1
Veizer J, Godderis Y, François LM (2000) Evidence for decoupling of atmospheric CO_2 and global climate during the Phanerozoic eon. Nature 408:698–701
Verpoorter C, Kutser T, Seekell DA, Tranvik LJ (2014) A global inventory of lakes based on high-resolution satellite imagery. Geophys Res Lett 41:6396–6402. https://doi.org/10.1002/2014GL060641
Von Blanckenburg F (2005) The control mechanisms of erosion and weathering at basin scale from cosmogenic nuclides in river sediment. Earth Planet Sci Lett 237:462–479
Wagreich M, Lein R, Sames B (2014) Eustasy, its controlling factors, and the limno-eustatic hypothesis—concepts inspired by Eduard Suess. Aust J Earth Scis 107:115–131
Wagreich M, Haq BU, Melinte-Dobrinescu MC, Sames B, Yilmaz I (2016) Advances and perspectives in understanding Cretaceous sea-level change. Palaeogeogr Palaeoclimatol Palaeoecol 441:391–392
Wallmann K (2001) Controls on Cretaceous and Cenozoic evolution of seawater composition, atmospheric CO_2 and climate. Geochim Cosmochim Acta 65:3005–3025
Wan C-B, Wang D-H, Zhu Z-P, Quan C (2011) Trend of Santonian (Late Cretaceous) atmospheric CO_2 and global mean land surface temperature: evidence from plant fossils. Sci China Earth Sci 54:1338–1345
Wang Y, Huang C, Sun B, Quan C, Wu J, Lin Z (2014) Paleo-CO_2 variation trends and the Cretaceous greenhouse climate. Earth Sci Rev 129:136–147
Waters CN, Zalasiewicz J, Summerhayes C, Barnosky AD, Poirier C, Gałuszka A, Cearreta A, Edgeworth M, Ellis EC, Ellis M, Jeandel C, Leinfelder R, McNeill JR, Richter DdeB, Steffen W, Syvitski J, Vidas D, Wagreich M, Williams M, Zhisheng A, Grinevald J, Odada E, Oreskes N, Wolfe AP (2016) The Anthropocene is functionally and stratigraphically distinct from the Holocene. Science 351:1–10
Wendler J, Wendler I (2016) What drove sea-level fluctuations during the mid-Cretaceous greenhouse climate? Palaeogeogr Palaeoclimatol Palaeoecol 441:412–419
Wendler J, Wendler I, Vogt C, Kuss J (2016) Link between cyclic eustatic sea-level change and continental weathering: evidence for aquifer-eustasy in the Cretaceous. Palaeogeogr Palaeoclimatol Palaeoecol 441:430–437
Wold CN, Hay WW (1993) Reconstructing the age and lithology of eroded sediment. Geoinformatics 4:137–144
Wold CN, Shaw CA, Hay WW (1993) Mass-balanced reconstruction of overburden. In: Harff J, Merriam DF (eds) Computerized basin analysis: the prognosis of energy and mineral resources. Plenum Press, New York, pp 115–130
Wolfe JA (1993) A method of obtaining climatic parameters from leaf assemblages. US Geol Surv Bull 2040:73
Wolfe JA (1995) Paleoclimatic estimates from Tertiary leaf assemblages. Annu Rev Earth Planet Sci 23:119–142
Zharkov MA, Murdmaa IO, Filatova NI (1998) Paleogeography of the Coniacian–Maastrichtian Ages of the Late Cretaceous. Stratigr Geol Correl 6/3:209–221
Ziegler AM, Scotese CR, Barrett SF (1982) Mesozoic and cenozoic paleogeographic maps. In: Brosche P, Sündermann J (eds) Tidal friction and earth's rotation II. Springer, Berlin, pp 240–252
Ziegler AM, Rowley DB, Lottes AL, Sahagian DL, Hulver ML, Gierlowski TC (1985) Paleogeographic interpretation: with an example from the Mid-Cretaceous. Ann Rev Earth Planet Sci 13:385–425